AMERICAN SOCIETY FOR MICROBIOLOGY | mBio

Check for updates

| Virology | Research Article

RAB5 is a host dependency factor for the generation of SARS-CoV-2 replication organelles

Yuexuan Chen,[1] Susanne Klute,[2] Konstantin Maria Johannes Sparrer,[2,3] Ruth Serra-Moreno[1]

AUTHOR AFFILIATIONS See affiliation list on p. 25.

ABSTRACT Severe acute respiratory syndrome coronavirus 2 (SARS-CoV-2) remains a threat due to the emergence of variants with increased transmissibility and enhanced escape from immune responses. Like other coronaviruses before, SARS-CoV-2 likely emerged after its transmission from bats. The successful propagation of SARS-CoV-2 in humans might have been facilitated by usurping evolutionarily conserved cellular factors to execute crucial steps in its life cycle, such as the generation of replication organelles—membrane structures where coronaviruses assemble their replication-transcription complex. In this study, we found that RAB5, which is highly conserved across mammals, is a critical host dependency factor for the replication of the SARS-CoV-2 genome. Our results also suggest that SARS-CoV-2 uses RAB5$^+$ membranes to build replication organelles with the aid of COPB1, a component of the COP-I complex, and that the virus protein NSP6 participates in this process. Hence, targeting NSP6 represents a promising approach to interfere with SARS-CoV-2 RNA synthesis and halt its propagation.

IMPORTANCE In this study, we sought to identify the host dependency factors that severe acute respiratory syndrome coronavirus 2 (SARS-CoV-2) uses for the generation of replication organelles: cellular membranous structures that SARS-CoV-2 builds in order to support the replication and transcription of its genome. We uncovered that RAB5 is an important dependency factor for SARS-CoV-2 replication and the generation of replication organelles, and that the viral protein NSP6 participates in this process. Hence, NSP6 represents a promising target to halt SARS-CoV-2 replication.

KEYWORDS COP-I, COPB1, NSP6, RAB5, replication organelle, SARS-CoV-2

The coronavirus disease 2019 (COVID-19) pandemic has evidenced that spillover episodes of viruses naturally infecting other animals are more frequent than in previous decades (1). Besides severe acute respiratory syndrome coronavirus 2 (SARS-CoV-2), six other human coronaviruses [NL63, 229E, OC43, HKU1, SARS-CoV, and Middle East respiratory syndrome-related coronavirus (MERS-CoV)] emerged in the 20th and 21st centuries, most likely because of cross-species transmission events from bats and rodents (2–4). Human activities like deforestation, intensive livestock production, and urbanization of the environment are drivers for the increased incidence of zoonotic infections (5, 6). While higher exposure to wild animals rises the probability of transmission of their viruses, these viruses must find a suitable environment in the new host to successfully cross the species barrier. This requires (i) an appropriate receptor for entry into the new host cells, (ii) ability to antagonize/evade the antiviral defenses in the new host, and (iii) being capable of hijacking the cellular machinery (dependency factors) of the new host in order to replicate (6–8). Here, we investigated the human dependency factors that SARS-CoV-2 utilizes to generate replication organelles (ROs), a critical step in the replication cycle of coronaviruses.

Invited Editor Paul Ahlquist, University of Wisconsin-Madison, Madison, Wisconsin, USA

Editor Stephen P. Goff, Columbia University Medical Center, New York, New York, USA

Address correspondence to Ruth Serra-Moreno, ruth_serra-moreno@urmc.rochester.edu.

The authors declare no conflict of interest.

See the funding table on p. 25.

Received 23 October 2024
Accepted 3 March 2025
Published 1 April 2025

Upon entry, coronaviruses synthesize the non-structural proteins (NSPs) that are responsible for the replication of their genome and production of subgenomic mRNAs, which allow the synthesis of their structural and accessory proteins. Among this first set of proteins, coronaviruses use NSP3, NSP4, and NSP6 to remodel cellular membranes and create ROs (9–13): double membrane vesicles (DMVs) where the virus replication-transcription complex (RTC) assembles (14). Most of the work on SARS-CoV-2 ROs has focused on understanding the virus molecules involved in DMV biogenesis. These studies found that while NSP3/4/6 are required to build ROs in most coronaviruses (9, 11–13), NSP3 and NSP4 are sufficient to generate DMVs in SARS-CoV-2, and that NSP6 participation is limited to increasing their number and organization, so they become functional replication factories (10). This role of NSP6 was confirmed using K22, a pan-NSP6 inhibitor that significantly reduced the number of DMVs and caused a defect in SARS-CoV-2 RNA yields (10). K22 was previously discovered in a screen for compounds against the human coronavirus 229E. Since only viruses harboring mutations in NSP6 replicated in the presence of this drug, it was concluded that K22 targets NSP6, and this was later confirmed for other coronaviruses (15). Of note, SARS-CoV-2 NSP6 also facilitates immune evasion (16, 17). However, it is unknown whether K22 impacts this activity.

Despite our increasing understanding of the virus genes involved in RO formation, the cellular origin of these replication factories is still a focus of debate. Endoplasmic reticulum (ER), Golgi, and autophagosomes have been proposed as membrane sources to generate SARS-CoV-2 ROs (11, 18–22). Structural studies revealed that these DMVs resemble autophagic membranes, suggesting that coronaviruses utilize elements of the autophagy machinery for RO biogenesis (23–29). However, autophagy has been found dispensable for the assembly of the SARS-CoV-2 RTC (10, 30). More recent studies have shown a physical connection between the SARS-CoV-2 ROs and zippered ER membranes, suggesting that ROs have an ER origin (10, 14, 31–33). Still, the dependency factors used by SARS-CoV-2 to create ROs, and whether ER membranes are their only source, remain largely unknown. Consistent with previous studies, here, we show that functional autophagy is dispensable for SARS-CoV-2 genome replication, and we identify RAB5 as a critical host dependency factor for SARS-CoV-2 ROs. RAB5 (Ras-associated protein RAB5A) is a GTPase crucial for the early steps of the endocytic pathway by facilitating vesicular transport, membrane trafficking, and signaling (34–37). Besides RAB5, our results indicate that SARS-CoV-2 builds ROs with the aid of COPB1 (COP-I coat complex subunit beta 1), a molecule of the COP-I complex, which participates in the retrograde transport from Golgi to the ER (38, 39). Finally, our studies suggest that the virus protein NSP6 recruits RAB5 and COPB1 for RO biogenesis. These conclusions have been derived from five main findings: (i) deletion of *RAB5* and *COPB1* significantly reduces SARS-CoV-2 RNA synthesis, (ii) *RAB5* deletion significantly impairs RO formation, (iii) NSP6 and the virus RNA-dependent RNA polymerase co-purify with the RAB5^{+} endosomal fraction, (iv) NSP6 associates with both RAB5 and COPB1, and (v) NSP6 facilitates an interaction between RAB5 and COPB1. Therefore, our findings reveal NSP6 as a promising target against SARS-CoV-2 and identify the endosomal and trafficking machinery as key contributors to the formation of ROs. Importantly, RAB5 and COPB1 are highly conserved in mammals (40). Hence, the use of such ubiquitous pathways might have contributed to the successful transmission of SARS-CoV-2 from its reservoir to humans.

RESULTS

SARS-CoV-2 RNA kinetics

To investigate the origins of the DMVs that SARS-CoV-2 uses for the assembly of the RTC, we first defined the time post-infection in which new virus RNA copies are synthesized, before progeny virions are detected. At this time, the virus-mediated remodeling of cellular membranes should have already materialized, with most products of genome replication [i.e., double-stranded RNA (dsRNA)] present in ROs (41–43). For this, we examined the RNA replication kinetics of an early SARS-CoV-2 isolate, Hong Kong (HK;

GenBank: MT547814) in different cell lines. African green monkey kidney epithelial VeroE6, human lung epithelial A549-ACE2, human lung fibroblast MRC5-ACE2, human kidney HEK293T-ACE2, and human bronchial epithelial 16HBE cells were infected with SARS-CoV-2 HK at a multiplicity of infection (MOI) of 1 in a synchronized manner by keeping infections for 1 h at 4°C. At 2, 4, 6, 8, 10, 16, 24, and 48 h post-infection, cells were harvested for RNA extraction. In parallel, culture supernatants were collected to measure virion production by tissue culture infectious dose 50 ($TCID_{50}$). SARS-CoV-2 genomic RNA was measured by reverse transcription followed by quantitative PCR (RT-qPCR) using primers specific for NSP12 (the catalytic subunit of the virus RNA-dependent RNA polymerase; RdRp) and NSP6, which both are part of *ORF1ab*, a reading frame only present in the full-length genomic RNA. qPCR primers for the host genes *GAPDH*, *ACTB,* and *CRT* were used for normalization and to ensure comparable input RNA across samples. SARS-CoV-2 genome replication was calculated as fold-change over basal virus RNA (detected at 2 h post-infection). New virus RNA copies were detected at 6 h post-infection for most cell lines—which aligns with the emergence of ROs (44, 45)—except for 16HBE cells. In this case, RNA replication was detected at 10 h post-infection (Fig. 1A). Hence, these findings indicate that the assembly of the virus RTC has already occurred by 6 h post-infection (10 h in 16HBE cells). This is consistent with an absence of infectious particle production at that time. In fact, cell-free infectious particles were first detected 8 h post-infection for most cells and at 24 h post-infection for 16HBE cells (Fig. 1B). Therefore, we selected 6 h post-infection as the time to examine the subcellular distribution of the RTC and to measure any defects in virus RNA synthesis in the presence of inhibitors for different cellular processes. For 16HBE cells, these assays were performed 10 h post-infection.

Autophagy is dispensable for SARS-CoV-2 RNA synthesis

To investigate whether SARS-CoV-2 uses autophagy to generate ROs, Vero E6 cells were infected with SARS-CoV-2 HK (MOI = 1), and the distribution of the RTC relative to autophagy membrane markers was examined by fluorescence microscopy at 6 h post-synchronized infection. SARS-CoV-2 dsRNA (as an intermediate product generated during genome replication) and the virus RdRp (NSP12) were used as markers for the RTC. Specificity for these markers was tested by staining uninfected cells. While no signal for dsRNA was detected in uninfected cells, cross-reactivity of the antibody used for the virus RdRp with nuclear factors was observed (Fig. S1). However, in infected cells, RdRp staining was also found in the cytoplasm (Fig. 2A, white, dotted area), which is the location where the virus polymerase is expected (46–48). Given the RdRp unspecific nuclear staining, we subsequently decided to label the RTC with dsRNA. Our assays showed little or no overlap between the RTC and EGFP-LC3B (Fig. 2A), an autophagosome marker (49), and this was confirmed by measuring the Pearson's correlation coefficient (*R*) (Fig. 2G). Similarly, little or no co-localization was observed between the virus RTC and phagophore (DFCP1) or omegasome (WIPI2) membranes markers (50, 51). Likewise, the autophagy receptor SQSTM1 (52, 53) distributed away from the virus RTC (Fig. 2B through D and G). Since previous work with the betacoronavirus murine hepatitis virus (MHV) uncovered that its RTC assembles in EDEMosomes (29), ER-derived vesicles that are coated with non-lipidated LC3, we investigated if SARS-CoV-2 uses a similar mechanism. However, no co-localization was detected between the RTC and the EDEMosome marker EDEM1 or endogenous LC3 (Fig. 2E through G). Here, we stained for the endogenous protein because that same study reported that EGFP-LC3B does not recapitulate the distribution of non-lipidated LC3 when coating EDEMosomes (29). Consistent with our findings in Vero E6 cells, no overlap between the virus RTC and endogenous LC3 was observed either in more physiologically relevant cells, such as A549-ACE2, MRC5-ACE2, and HEK293T-ACE2 (Fig. S2). Hence, these findings indicate that the SARS-CoV-2 RTC does not localize to autophagy-associated membranes.

To confirm that autophagy is dispensable for RO formation, we blocked autophagy by generating *ATG5* knockout cells in VeroE6, A549-ACE2, MRC5-ACE2, and HEK293T-ACE2

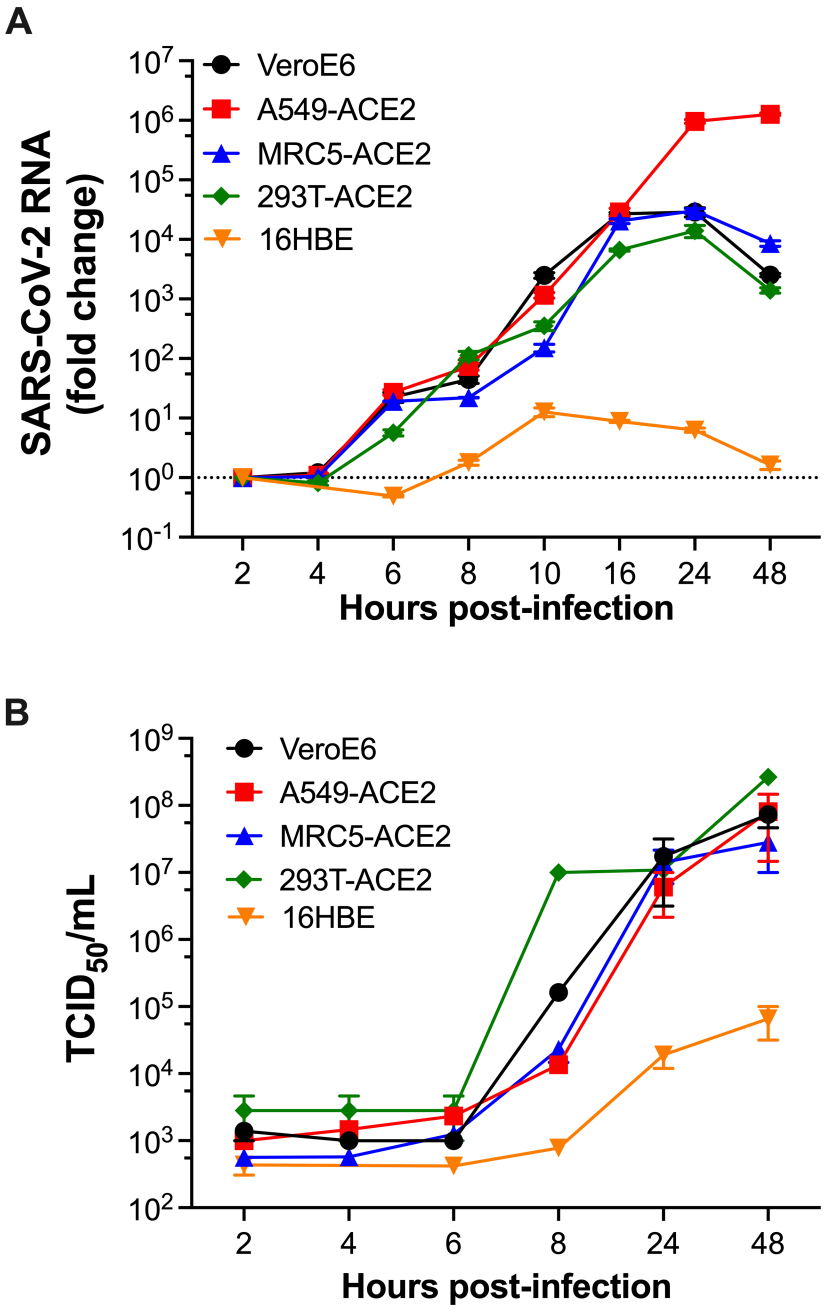

FIG 1 RNA replication kinetics of SARS-CoV-2. (A) VeroE6, A549-ACE2, MRC5-ACE2, HEK293T-ACE2, and 16HBE cells were synchronously infected with SARS-CoV-2 HK at MOI = 1. Total RNA was extracted at the selected time points, converted to cDNA by reverse transcription, and virus genome copies were measured by qPCR using primer pairs specific for *NSP12* and *NSP6*. Changes in SARS-CoV-2 RNA levels were normalized to the first time point and expressed as fold-change. Dotted line represents basal virus RNA counts. (B) The culture supernatants from these infections were collected at the selected time points to measure the degree of virion production by $TCID_{50}$ on VeroE6 cells. Data correspond to the mean and SEM of three independent experiments.

cells. *ATG5* was targeted because it is critical for autophagy progression and autophagosome biogenesis (54, 55). *ATG5* knockout was verified by western blot from pooled cells, showing undetectable levels of the protein and a defect in the emergence of LC3-II (Fig. S3A)—a hallmark of a defect in *ATG5* (56, 57). The effect of *ATG5* knockout on SARS-CoV-2 RNA counts was investigated by RT-qPCR at 2 and 6 h post-infection to assess whether

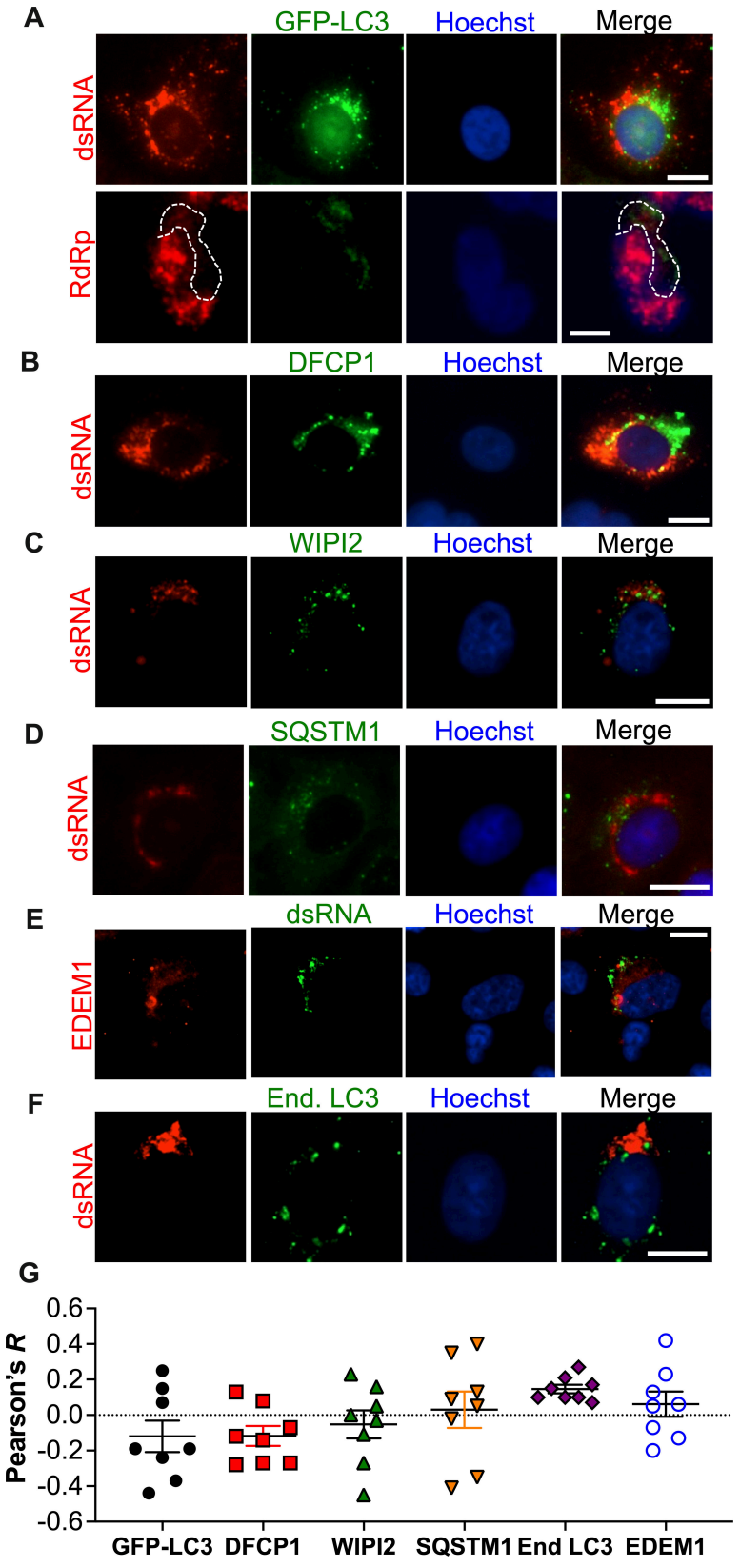

FIG 2 Autophagy membranes do not overlap with the SARS-CoV-2 RTC. (A–F) VeroE6 cells were infected with SARS-CoV-2 HK (MOI = 1) in a synchronized manner. Six hours later, cells were stained for the virus dsRNA and/or RdRp and different autophagy markers. Images: representative pictures from

(Continued on next page)

Fig 2 (Continued)

three independent experiments for the relative distribution between SARS-CoV-2 dsRNA and/or RdRp and autophagosomes (EGFP-LC3B), phagophores (DFCP1), omegasomes (WIPI2), autophagy receptors (SQSTM1), EDEMosomes (EDEM1), and endogenous LC3. Dotted white lines: delineation of cellular cytoplasm. White scale bar: 10 µm. (G) Graph: the Pearson's correlation coefficient (*R*) value for the co-localization of SARS-CoV-2 dsRNA with the indicated markers was calculated from eight randomly selected fields. Data correspond to raw values, their mean, and SEM.

ATG5 deletion causes any defects in genome replication due to impacting virus uptake. To facilitate data interpretation, RT-qPCR data are expressed as the inverse value of the raw Cq (1/Cq), with no normalization, but RT-qPCR for cellular *GAPDH*, *ACTB,* and *CRT* confirmed comparable input RNA across samples. The reasoning for presenting the data in this format is that the Cq values for the virus RNA earlier in the infection are higher than when genome replication is occurring. So, plotting the raw Cq would have given the impression that there is a decrease in RNA levels over time. Through this method, we can see the magnitude of the impact (if any) that knocking out *ATG5* has on genome replication. Nevertheless, because this is an unusual presentation of qPCR data, this information is also provided as fold-change over parental cells using the $2^{\Delta\Delta Cq}$ factor (Fig. S4A). Deletion of *ATG5* had no negative impact on SARS-CoV-2 RNA uptake, since the Cq values were comparable between the respective parental and *ATG5*KO cells at 2 h post-infection (Fig. S3A, open circles). Similarly, *ATG5* deletion had no effect on virus RNA synthesis in any of the cell types investigated at 6 h post-infection or at later time points (Fig. S3A and S4A). In *ATG5*KO A549-ACE2 cells, however, RNA yields were reduced at 24 h post-infection. Since no defect in RNA synthesis was observed in these cells at 6 h post-infection, we concluded that autophagy is important for late steps of the virus life cycle in this cell line, like virion assembly and/or egress. This is consistent with reduced virus RNA counts 24 h post-infection, which would correspond to ~3 replication cycles.

To further rule out a role for autophagy in RO biogenesis, we used the following autophagy-modulating compounds: 3-MA (class III PI3K inhibitor with transient activity on class I PI3K), VPS34IN (class III PI3K inhibitor), torin2, vistusertib (mTOR inhibitors), dactolisib (PI3K [p110α/γ/δ/β] and mTOR inhibitor), and wortmannin (class I, class II, and class III PI3K inhibitor). Compared to dimethyl sulfoxide (DMSO) (D on the *x*-axis), none of these compounds caused major impacts on virus RNA counts at 6 h post-infection, since any fluctuations in RNA levels never reached a twofold-change (58) (Fig. S3B through G). Only 3-MA and VPS34IN reduced virus RNA synthesis at concentrations much higher than their 50% inhibitory concentration (IC_{50}) dose for autophagy inhibition (Fig. S3F and G). Importantly, no cytotoxicity was caused by either of these drugs at these concentrations (Fig. S3H), suggesting that their impact on virus RNA may be due to pleiotropic effects. Overall, our findings support that autophagy is dispensable for SARS-CoV-2 RNA synthesis.

The SARS-CoV-2 RTC co-localizes with RAB5$^+$ membranes

After ruling out a role for autophagy in RO formation, we examined the subcellular distribution of the virus RTC relative to several intracellular membrane markers. The reasoning is that the presence of cellular proteins on the RO surface could be indicative of their membrane origin. For this, we took an unbiased approach and used markers for several intracellular membranes, including early endosomes (RAB5), late endosomes (CD63), recycling endosomes (RAB11), *cis*-Golgi (GOSR1), *trans*-Golgi (TGN46), exosomes (CD81), ER (calnexin), lipid droplets (ADRP), and mitochondria (MitoTracker). As a control, the distribution of these cellular markers in the absence of infection was also examined (Fig. S5). VeroE6 cells were infected with SARS-CoV-2 HK (MOI = 1), and 6 h later, cells were stained for the virus dsRNA and the intracellular markers specified above. Little co-localization was observed between the virus dsRNA and recycling endosomes, exosomes, late endosomes, and the ER markers, with Pearson's correlation coefficients between 0.1 and 0.3. Some degree of co-localization was detected with Golgi (TGN46),

lipid droplets, and mitochondrial markers, with Pearson's values between 0.5 and 0.6. However, the strongest co-localization was observed with the early endosomal marker (RAB5), with an average Pearson's correlation coefficient of 0.8 (Fig. 3), which was significantly higher than the co-localization observed for TGN46, ADRP, and mitochondria. Similar results were obtained when infected cells were stained for the viral RdRp as a proxy for the RTC (Fig. S6). Remarkably, upon infection, we noticed that some of these intracellular markers, especially RAB5 and TGN46, appear more intense and dispersed throughout the cytosol, which likely reflects that the infection is triggering these changes (Fig. S7). In fact, it has been shown that SARS-CoV-2 promotes Golgi fragmentation, reshapes the cytoskeleton, and causes *RAB5* mRNA upregulation in COVID-19 patients (31, 59, 60), so our findings are in line with those reports. Overall, our assays reveal that the virus RTC primarily overlaps with RAB5, suggesting that the virus uses endosomal membranes to build ROs or that it recruits RAB5 to the RO membrane.

RAB5$^+$ early endosomes are required for the biogenesis of SARS-CoV-2 ROs

Because RAB5 is the marker that most strongly co-localized with the virus RTC, and this strong co-localization was corroborated in the other cells used in this study (Fig. S8), we explored the role of early endosomes in SARS-CoV-2 genome replication. For this, we used the inhibitors pitstop2 and dynasore. Pitstop2 inhibits clathrin oligomerization with adaptor proteins, which impacts the maintenance of the early endosomal population by interfering with vesicular transport from the plasma membrane and Golgi (61–64). Dynasore inhibits dynamins, which are involved in fission events during receptor-mediated endocytosis. Hence, the use of pitstop2 and dynasore could help us understand what process of early endosome biogenesis is important for SARS-CoV-2 genome replication. Importantly, besides fusion at the plasma membrane, SARS-CoV-2 can enter target cells by receptor-mediated endocytosis, and the selection between these two modes of entry is dictated by the presence of transmembrane serine protease 2 (TMPRSS2) on the cell surface as well as mutations accumulated in the Spike of certain SARS-CoV-2 variants (65–68), which favor fusion at endosomes. Although the HK variant uses membrane fusion as the entry mechanism (65), we wanted to exclude any impact these inhibitors might have on entry, which would consequently affect virus RNA synthesis. Since our kinetics assay showed that new genome copies are detectable by 6 h post-infection (Fig. 1A), drugs were added 4.5 h after synchronized infection, so we could influence RO formation without impacting entry. Consistent with the distribution of the virus RTC at RAB5$^+$ early endosomes, pitstop2 significantly reduced virus RNA synthesis. However, dynasore had only a minor impact (Fig. 4A), which varied across cell lines, suggesting that endosomes from endocytic vesicles play a secondary role in SARS-CoV-2 RNA synthesis. To rule out that pitstop2's impact on virus RNA is not due to toxicity, the effects of this compound on host transcription (*GAPDH* mRNA), RNA synthesis from ectopic DNA [green fluorescent protein (GFP)-coding plasmid], and cell viability were assessed by RT-qPCR and XTT assays. These assays showed no defects in host or ectopic mRNA synthesis nor evidence of cytotoxicity (Fig. 4B).

The role of RAB5 in SARS-CoV-2 RNA synthesis was confirmed by generating *RAB5* knockout cells. To assess for any effects that deleting *RAB5* might exert on virus entry, we examined for differences in virus RNA at 2 and 6 h post-synchronized infection between parental and *RAB5*KO cells. As for the *ATG5*KO assays, qPCR data are expressed as the inverse value of the raw Cq (1/Cq), but these data are also presented as fold-change over parental cells in Fig. S4B. Deletion of *RAB5* did not delay virus entry, since virus RNA counts in *RAB5*KO cells were similar or higher than parental cells at 2 h post-infection (Fig. S4B and S9A). However, deletion of *RAB5* significantly impaired SARS-CoV-2 RNA synthesis in all cells investigated (Fig. 4C; Fig. S4B and S9A, black circles). To further exclude a possible impact of deleting *RAB5* on virus replication due to a defect in virus entry, we used an entry reporter assay. For this, we infected parental and *RAB5*KO HEK293T-ACE2-30F-PLP2 cells with SARS-CoV-2 HK at MOIs = 2 and 5, and cells were analyzed 4 h post-infection. HEK293T-ACE2-30F-PLP2 cells are engineered

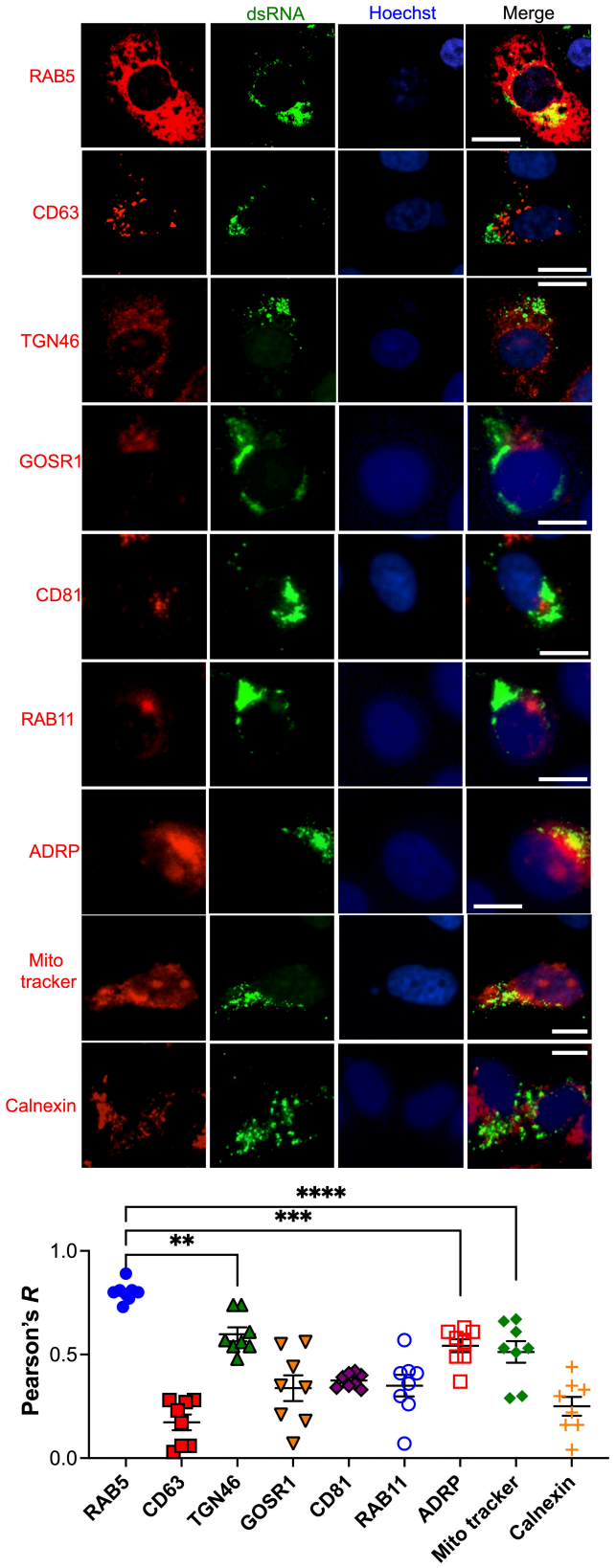

FIG 3 Early endosomal membranes highly co-localize with SARS-CoV-2 dsRNA. VeroE6 cells were infected with SARS-CoV-2 HK (MOI = 1) in a synchronized manner. Six hours later, cells were fixed,

(Continued on next page)

Fig 3 (Continued)

blocked, and stained for the virus dsRNA and the intracellular markers RAB5, CD63, TGN46, GOSR1, CD81, RAB11, ADRP, MitoTracker, and calnexin. Images: representative pictures of three independent experiments. White scale bar: 10 µm. Graph: the Pearson's correlation coefficient (*R*) value for the co-localization of SARS-CoV-2 dsRNA and the intracellular markers listed above was calculated from eight randomly selected fields. Raw values with their mean and SEM are represented. **, $P < 0.01$; ***, $P < 0.001$; ****, $P < 0.0001$.

to constitutively express renilla luciferase and a SARS-CoV-2 PLpro-activatable firefly luciferase, which allow to measure infectivity (69) (Fig. S9B, cartoon). Because SARS-CoV-2 PLpro is a non-structural protein encoded within *ORF1ab*, which is expressed without the need of generating ROs, this cell line allows us to measure virus entry and whether knocking out *RAB5* has an impact on it. No differences in firefly luciferase activation were observed between parental and *RAB5*KO cells, regardless of the MOI used (Fig. S9B), further supporting that RAB5 is dispensable for SARS-CoV-2 HK entry but is required for the replication of its genome. These quantitative measurements are empirically supported by fluorescence microscopy, where *RAB5* deletion caused a severe loss in products of virus genome replication like dsRNA. In fact, the only cells with dsRNA staining happened to have some residual RAB5 expression (Fig. 4D, yellow arrowhead). Accordingly, reconstitution of RAB5 into *RAB5*KO cells rescued the phenotype (Fig. 4D, bottom). To confirm a role for RAB5 in the formation of ROs, transmission electron microscopy (TEM) images were obtained from parental and *RAB5*KO VeroE6 cells. For this, cells were infected with SARS-CoV-2 HK at MOI = 5. Six hours later, cells were processed for TEM along with uninfected cells to confirm that juxtaposed DMVs are only observed under conditions of infection (Fig. S10). Unlike the infected parental cells, where several DMVs adjacent to each other were observed (Fig. 4E, top, white arrowheads), *RAB5*KO-infected cells displayed notably less DMVs (Fig. 4E, bottom, yellow arrow), and many maze-like membranous structures (Fig. 4E, bottom, yellow square), suggesting initiation of membrane remodeling, but failure to generate ROs. Quantification of DMVs and maze-like structures from 14 to 17 cells per experimental condition confirmed that deletion of *RAB5* causes a significant defect in RO formation and ruled out possible membrane artifacts due to deleting *RAB5* (Fig. 4F and G). Overall, our results indicate that clathrin-dependent $RAB5^+$ early endosomes are required for SARS-CoV-2 genome replication and RO biogenesis.

COPB1 is necessary for SARS-CoV-2 RNA synthesis

To examine the role of factors involved in the trafficking of early endosomes in SARS-CoV-2 RNA replication, we depleted AP1, AP2, and COPB1, a component of the COP-I complex, using silencing RNA (siRNA). We also used a dominant-negative mutant of VPS4 ($VPS4_{E228Q}$), an essential molecule for the function of the ESCRT (endosomal sorting complexes required for transport) machinery (70–72). Because of their higher transfection efficiency, here, we infected HEK293T-ACE2 cells that were previously transfected with these siRNAs and/or constructs. Depletion of these trafficking components as well as the expression of $VPS4_{E228Q}$ were verified by western blot (Fig. 5A, blots). While depletion of AP1 and AP2 or blocking the ESCRT machinery had no major impact on SARS-CoV-2 RNA synthesis, the depletion of COPB1 caused a significant defect in virus genome replication (Fig. 5A). These findings were reproduced in 16HBE *COPB1*KO cells (Fig. 5B). To exclude any potential effects that knocking out *COPB1* might have on virus entry, virus RNA counts were compared between parental and *COPB1*KO 16HBE cells at 6 and 10 h post-infection, since RNA synthesis is not detected until 10 h post-infection in these cells. No differences in total RNA counts were observed at 6 h post-infection, reflecting no defects in entry (Fig. S4C and S9C). This was also corroborated in *COPB1*KO HEK293T-ACE2-30F-PLP2 cells (Fig. S9D). In contrast, a significant reduction in total RNA counts was detected at 10 h post-infection (Fig. S4C and S9C), further supporting that COPB1 is important for SARS-CoV-2 RNA synthesis. In line with this, 16HBE cells treated

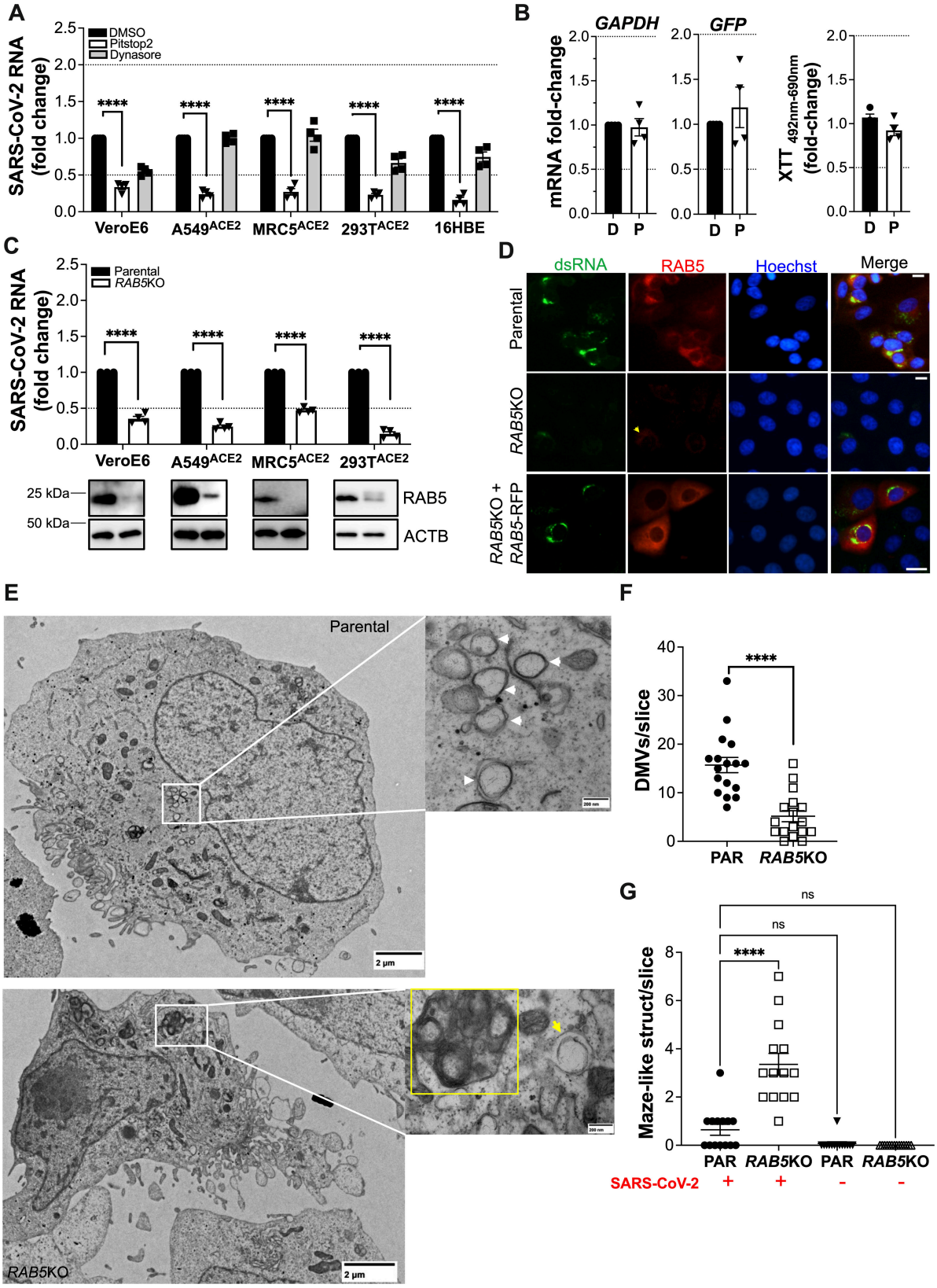

FIG 4 Clathrin and RAB5 are necessary for SARS-CoV-2 RNA synthesis and RO formation. (A) VeroE6, A549-ACE2, MRC5-ACE2, HEK293T-ACE2, and 16HBE cells were infected with SARS-CoV-2 HK (MOI = 1) in a synchronized manner. 4.5 h post-infection (8.5 h for 16HBE), cells were incubated with DMSO, pitstop2 (100 µM), or dynasore (80 µM) for 1.5 h. Their effect on virus RNA synthesis was examined by RT-qPCR, using primer pairs for *NSP12* and *NSP6*. SARS-CoV-2 RNA levels were

(Continued on next page)

Fig 4 (Continued)

expressed as fold-change after normalization with DMSO-treated cells. (B) The effect of DMSO (D) and pitstop2 (P) on mRNA levels of *GAPDH* or ectopic DNA (GFP provided by transfection) was investigated by adding 100 µM of the drug to VeroE6 cells for 1.5 h. Cells were harvested, RNA extracted, converted to cDNA, and analyzed by qPCR. Data are expressed as fold-change over DMSO. The impact of 6 h incubation of pitstop2 on cell viability was assessed by XTT assays. Data are expressed as fold-change over DMSO. Data correspond to the mean and SEM of four independent experiments. (C) Parental and *RAB5*KO VeroE6, A549-ACE2, MRC5-ACE2, and HEK293T-ACE2 cells were infected with SARS-CoV-2 HK (MOI = 1) in a synchronized manner. Six hours post-infection, total RNA was collected. SARS-CoV-2 genome copy numbers were determined by RT-qPCR using primer pairs for *NSP12* and *NSP6* and expressed as fold-change after normalization with the parental cells. Blots underneath confirm the depletion of RAB5. ACTB/β-actin is used as a housekeeping gene. Data correspond to the mean and SEM of four independent experiments. (D) Representative images of parental VeroE6, VeroE6 *RAB5*KO, and VeroE6 *RAB5*KO + RAB5 RFP cells infected with SARS-CoV-2 HK (MOI = 1) and stained 6 h post-infection for the virus dsRNA (green), RAB5 (red), and the nuclei (blue). White scale bar: 10 µm. (E) Parental VeroE6 (top) and *RAB5*KO VeroE6 cells (bottom) were infected with SARS-CoV-2 HK at MOI = 5 in a synchronized manner. Six hours later, cells were fixed for transmission electron microscopy processing. The presence of double membrane vesicles (DMVs) is depicted with white and yellow arrowheads. Areas delineated in white squares are shown at a higher magnification in the right panels. Incomplete DMVs are found within yellow squares. Scale bars: 2 µm and 200 nm. Images are representative of three independent experiments. (F, G) The quantification of DMVs per cell (F) as well as maize-like structures (G) for >14 cells is provided for each experimental condition (parental and *RAB5*KO cells). Raw values with their mean and SEM are represented. ****, $P < 0.0001$; ns, not significant.

with brefeldin A or golgicide, inhibitors of the COP-I complex (73–77), showed a drastic reduction of SARS-CoV-2 RNA counts (Fig. 5C). These observations were empirically confirmed by fluorescence microscopy, where deletion of *COPB1* dramatically impacted the accumulation of virus RNA replication products (dsRNA, Fig. 5D). Therefore, these assays confirm a role for the COP-I machinery in the replication of the SARS-CoV-2 genome.

SARS-CoV-2 NSP6 associates with RAB5 and COPB1

Together with NSP3 and NSP4, NSP6 is an ER, multipass transmembrane coronavirus protein critical for the creation and maintenance of replication organelles (9–13). In fact, the sole co-expression of NSP3, NSP4, and NSP6 induces membrane remodeling and DMVs as the ones observed during coronavirus infection (9, 10, 78, 79). However, in the absence of NSP3 and NSP4, NSP6 only induces membrane zippering, and these rearrangements are not sufficient to trigger RO formation (10, 16). Importantly, a recent study found that when expressing tagged NSP6 in the absence of NSP3 and NSP4, the location of the tag (N-terminus vs C-terminus) can drastically affect its subcellular distribution (10). Consistent with that report, we found that N-terminally tagged NSP6 displays a puncta distribution (Fig. 6A, top), while C-terminally tagged NSP6 shows a reticular and perinuclear localization (Fig. 6A, bottom). This reticular distribution of NSP6 tagged at the C-terminus has already been observed for other coronaviruses, where it was concluded that NSP6 resides in the ER (27). In contrast, we found that NSP6 had a similar distribution phenotype regardless of where the tag was attached when expressed in infected cells (where NSP3 and NSP4 are present) (Fig. 6B), and this pattern is more similar to that of the C-terminally tagged NSP6 (Fig. 6A and B). Because NSP3 and NSP4 remodel cellular membranes that are later reorganized by NSP6 (10), one could envision a scenario where NSP6 is recruited to these sites to help in DMV organization, which likely contributes to the correct localization of the protein regardless of its tag location. Overall, these data further reinforce the need of NSP3/4/6 for successful RO formation.

Unlike NSP3 and NSP4, NSP6 is more amenable to visualization and detection (80), so we investigated its role in recruiting RAB5$^+$ membranes. For this, our SARS-CoV-2 NSP6-HA construct is either co-transfected along with its NSP3 and NSP4 counterparts or transfected in infected cells to ensure proper subcellular distribution. Using this approach, we confirmed that both NSP6-HA and NSP6 produced during infection share a similar subcellular distribution, which co-localizes with the virus RTC (Fig. 6B and 7A, respectively). Accordingly, NSP6-HA co-immunoprecipitates with the virus RdRp (Fig. 7B), and in line with the extensive co-localization between the virus RTC and RAB5$^+$ membranes, both NSP6-HA and the virus RdRp co-purify with the early endosomal fraction (Fig. 7C), further supporting that SARS-CoV-2 uses early endosomes to build ROs and that

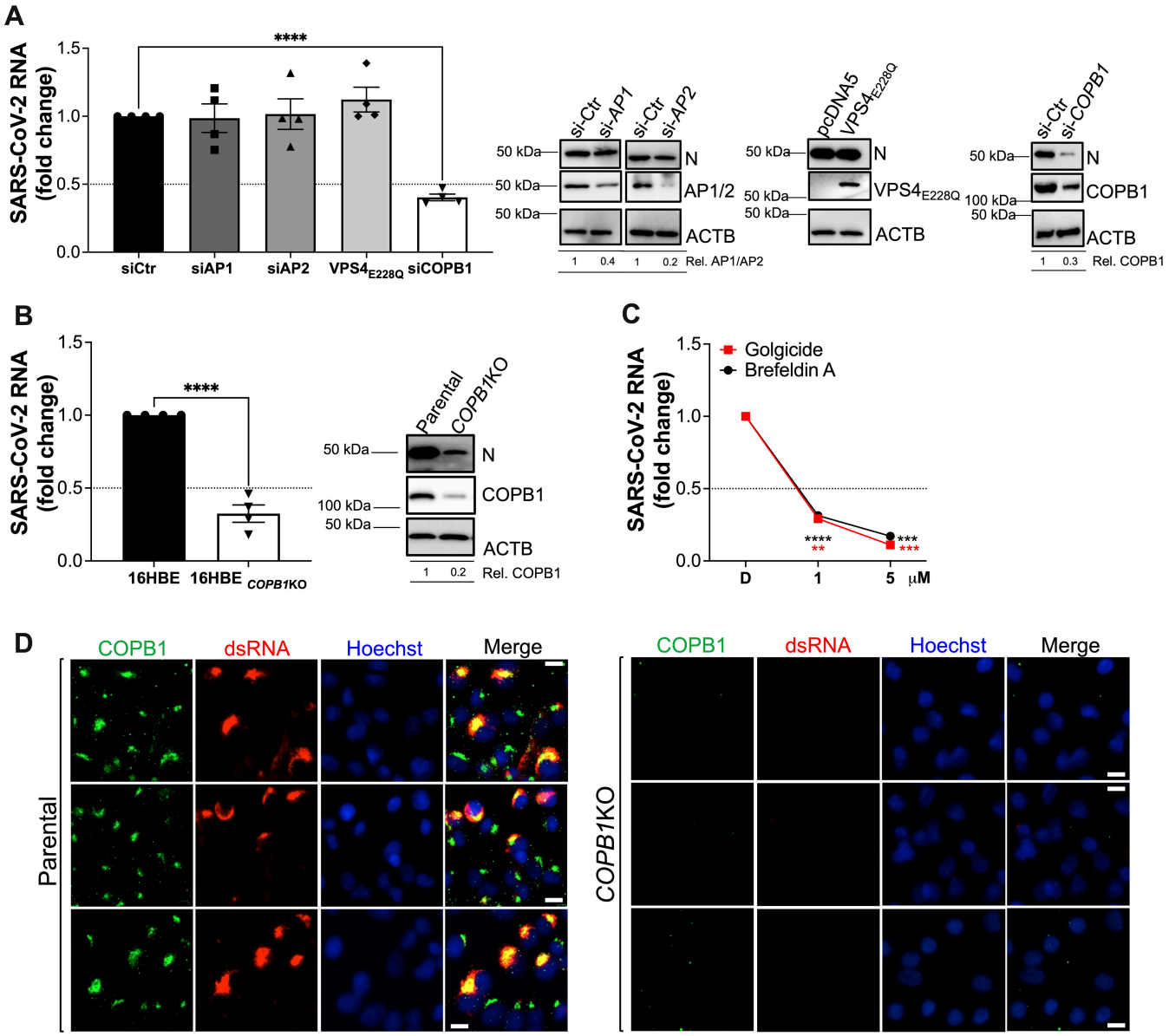

FIG 5 COPB1 is required for SARS-CoV-2 RNA synthesis. (A) HEK293T-ACE2 cells were transfected with siRNAs for AP1, AP2, and COPB1. To block the ESCRT machinery, cells were transfected with the VPS4 dominant-negative mutant $VPS4_{E228Q}$. The effect of depleting or blocking these vesicular trafficking molecules on SARS-CoV-2 RNA synthesis was determined by RT-qPCR using primer pairs for *NSP12* and *NSP6* and expressed as fold-change after normalization with the siRNA control. For $VPS4_{E228Q}$, data were normalized with an empty vector. Right panel shows representative blots to confirm the depletion or expression of the constructs indicated above. ACTB was used as a housekeeping gene. The impact of the depletion/expression of these constructs on the levels of SARS-CoV-2 late genes (i.e., nucleocapsid, N) was also examined. Relative expression levels are provided underneath the blots. (B) Parental 16HBE and *COPB1*KO cells were infected with SARS-CoV-2 HK (MOI = 1) in a synchronized manner. Ten hours post-infection, cells were harvested, and total RNA was collected. SARS-CoV-2 genome copy numbers were determined by RT-qPCR and expressed as fold-change after normalization with the parental cells. (C) The effect of COP-I inhibitors, golgicide and brefeldin A, on SARS-CoV-2 RNA synthesis was investigated in 16HBE cells after synchronized infection with SARS-CoV-2 HK (MOI = 1). Cells were treated 2 h post-infection at the indicated concentrations for 8 h prior to RNA extraction. SARS-CoV-2 genome copy numbers were determined by RT-qPCR and expressed as fold-change after normalization with DMSO (D on the *x*-axis). Data correspond to the mean and SEM of four independent experiments. **, $P < 0.01$; ***, $P < 0.001$; ****, $P < 0.0001$. (D) Representative fluorescence microscopy pictures of parental and *COPB1*KO A549-ACE2 cells infected with SARS-CoV-2 and stained for COPB1 (green) and the virus dsRNA (red). White scale bar: 10 µm.

NSP6 distributes at these locations. The role of NSP6 in SARS-CoV-2 RNA synthesis has previously been confirmed using K22, a compound that specifically disables NSP6 (10, 15), and we further corroborated those findings showing that K22 causes a

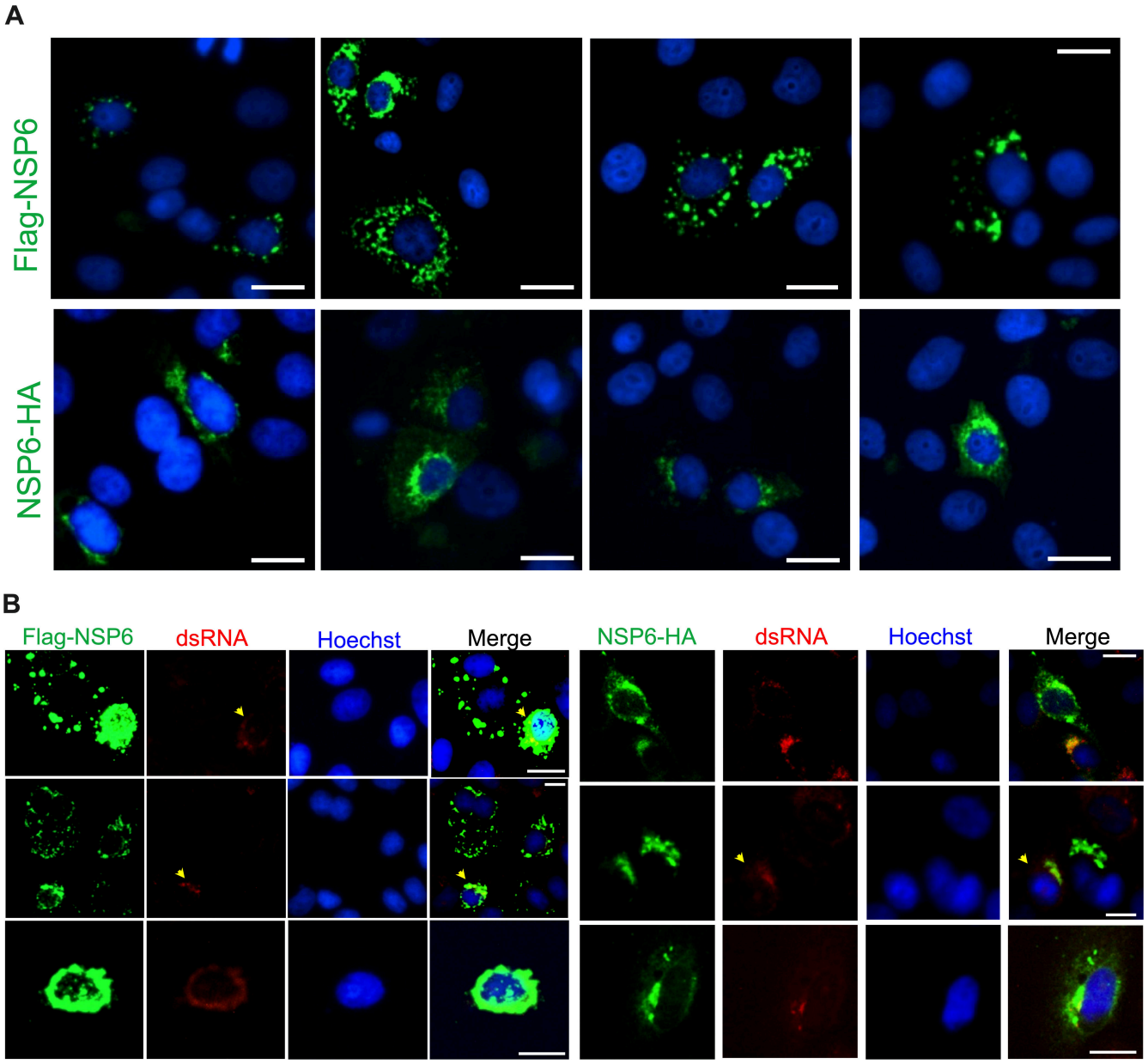

FIG 6 Tag location within NSP6 changes its distribution pattern, but its localization is restored in the context of infection. (A) Cellular distribution of Flag-NSP6 (top) and NSP6-HA (bottom) was investigated by fluorescence microscopy in VeroE6 cells. Cells are stained for Flag or HA (green) and the nucleus (blue). (B) VeroE6 cells were transfected with either Flag-NSP6 (left) or NSP6-HA (right) 1 day before infection with SARS-CoV-2 HK (MOI = 1). NSP6 distribution pattern was examined by fluorescence microscopy 6 h post-infection. Cells are stained for Flag or HA (green), the virus dsRNA (red), and the nucleus (blue). Yellow arrowheads indicate infected cells. White scale bar: 10 µm. Images are representative of three independent experiments.

dose-dependent defect in virus RNA counts (Fig. 7D). Of note, XTT assays using 80 µM of K22 ruled out any cytotoxic effects (Fig. 7E).

After confirming its relevance in SARS-CoV-2 RNA synthesis, we explored a potential role for NSP6 in recruiting RAB5 and COPB1 for the formation of ROs through immunoprecipitation (IP) and fluorescence microscopy of cells transfected with SARS-CoV-2 NSP6-HA or truncation mutants of this protein—along with NSP3 and NSP4. Here, NSP6 domains facing the cytoplasm (the regions more likely to interact with RAB5 and/or COPB1) were removed. We found that NSP6 co-immunoprecipitates with RAB5 (Fig. 8A) and distributes at RAB5$^+$ locations (Fig. 8B), and that deletion of the C-terminal domain of NSP6 causes its mislocalization away from RAB5 (Fig. 8C and D), suggesting that the

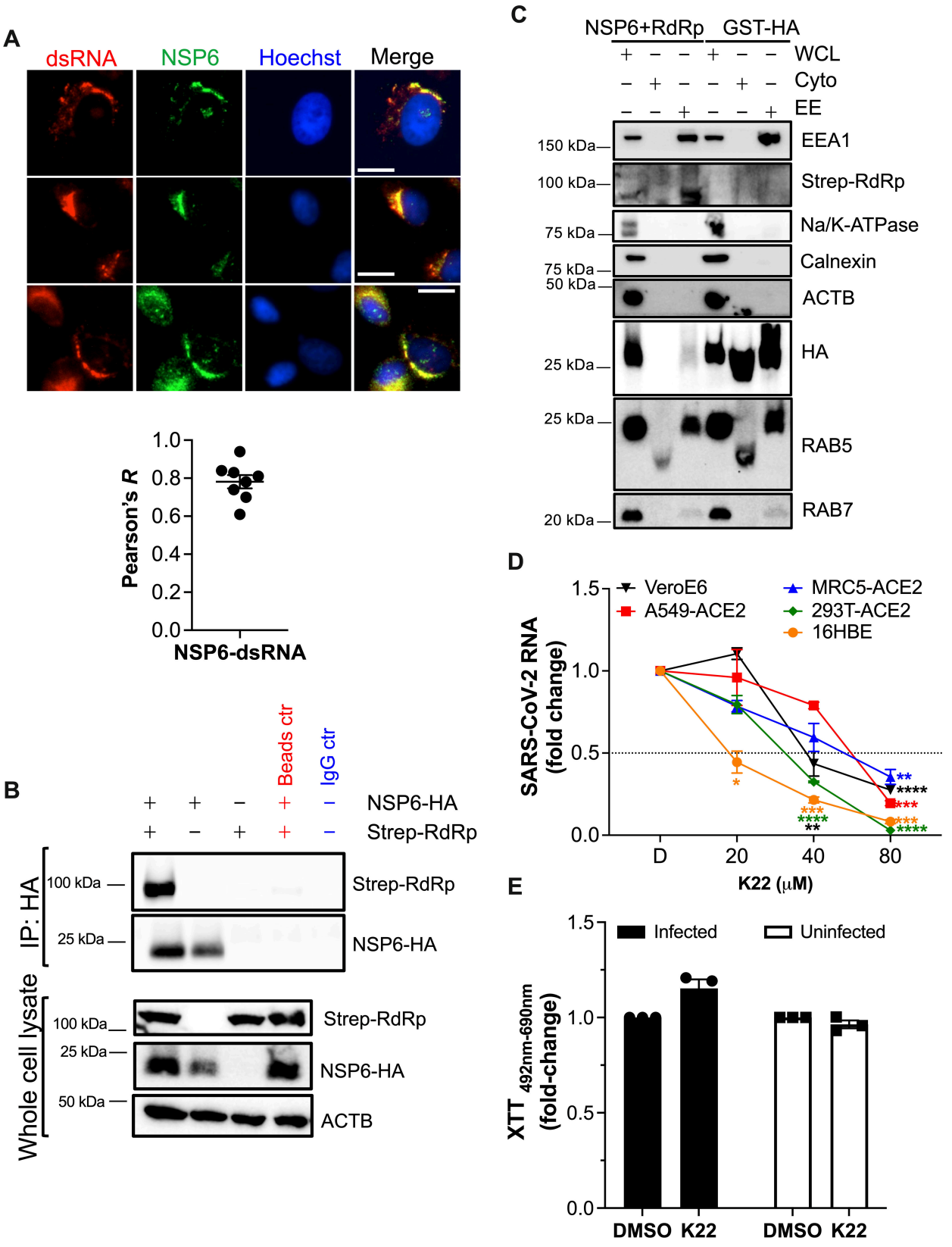

FIG 7 NSP6 co-localizes, interacts, and co-purifies with the virus RTC and is necessary for SARS-CoV-2 RNA synthesis. (A) VeroE6 cells were infected with SARS-CoV-2 HK (MOI = 1) in a synchronized manner. Six hours later, cells were fixed, blocked, and stained for the nuclei (blue), NSP6 (green), and dsRNA (red). Pictures are representative of three independent experiments. White scale bar: 10 µm. Graph: the Pearson's correlation coefficient (*R*) value for the co-localization

(Continued on next page)

Fig 7 (Continued)

of dsRNA and NSP6 was calculated from eight randomly selected fields. Individual values, their mean, and SEM are shown. (B) HEK293T cells were co-transfected with constructs coding for NSP3, NSP4, NSP6-HA, and Strep-RdRp. Forty-eight hours later, lysates were immunoprecipitated against NSP6-HA, and membranes were probed for Strep-RdRp. Lysates were also analyzed for RdRp, NSP6, and ACTB. Data are representative of three independent experiments. (C) Similar transfections were performed to investigate the presence of the virus RTC and NSP6 in early endosomal membranes by subcellular fractionation. Glutathione S-transferase (GST) was used as a control present in the cytosol and endosomes. Purity of the fractions was confirmed using antibodies against specific early endosomal markers (RAB5, EEA1), late endosomal markers (RAB7), cytosolic markers (non-prenylated RAB5), plasma membrane markers (Na/K ATPase), ER markers (calnexin), and cytoskeleton markers (ACTB). Low presence of RAB7 in the early endosomal fraction is expected, as the transition from early to late endosomes requires a RAB cascade where RAB5 and RAB7 temporarily co-exist. WCL, whole cell lysate. EE, early endosomal fraction. Cyto, cytosolic fraction. Data are representative of three independent experiments. (D) VeroE6, A549-ACE2, MRC5-ACE2, HEK293T-ACE2, and 16HBE cells were infected with SARS-CoV-2 HK (MOI = 1) in a synchronized manner. Increasing concentrations of the NSP6 inhibitor K22 were added 2 h post-infection. Four hours later (8 h for 16HBE cells), cells were harvested, total RNA was extracted, and the SARS-CoV-2 genome copy numbers were determined by RT-qPCR using primer pairs for *NSP12* and *NSP6*. The effect of K22 on virus RNA synthesis was expressed as fold-change after normalizing to DMSO (D on the *x*-axis). (E) The impact of K22 at 80 µM on cellular viability and toxicity was examined by XTT assays in both infected and uninfected VeroE6 cells and is expressed as fold-change over DMSO. *, $P < 0.05$; **, $P < 0.01$; ***, $P < 0.001$; ****, $P < 0.0001$. Data correspond to the mean and SEM of three independent experiments.

C-terminus of NSP6 is important for its association with RAB5. Similarly, NSP6 was found to co-immunoprecipitate with COPB1 (Fig. 9A). In this case, the NSP6 N-terminus seems to be involved in this interaction, since its truncation causes NSP6 to localize away from COPB1 (Fig. 9B and C). Importantly, our data do not exclude the participation of NSP3 and NSP4 in RAB5 and COPB1 recruitment, and given their concerted actions with NSP6, it is likely that they are also involved to some extent. Also, while our immunofluorescence images indicate that NSP6 uses its C-terminus to co-localize with RAB5 and that it uses its N-terminus to co-localize with COPB1, this technique does not have the resolution to assess protein-protein interactions. We tried to address this by co-immunoprecipitation. Unfortunately, some of the NSP6 truncation mutants were unspecifically being pulled down in their respective bead controls, so we could not reliably make conclusions about their binding with RAB5 or COPB1.

Finally, we used co-IP to explore whether NSP6 enhances an association between COPB1 and RAB5. While there seems to be minimal binding between these two proteins in the absence of NSP6, NSP6 enhanced their interaction (Fig. 10A). In line with this result, their degree of co-localization was significantly higher in infected cells (Fig. 10B and C). Overall, our findings indicate that $RAB5^{+}$ membranes are a source for SARS-CoV-2 ROs and that NSP6 participates in their recruitment, likely by facilitating an association between RAB5 and COPB1.

DISCUSSION

SARS-CoV-2 is the seventh coronavirus infecting humans. As for other human coronaviruses, SARS-CoV-2 likely emerged from a bat coronavirus (81–83) and quickly spread among the human population, suggesting that, besides finding an appropriate receptor for entry and being capable of evading/antagonizing the human antiviral defenses, the virus needed little adaptation after the spillover event. A possible explanation might be that the virus utilizes cellular factors that are widely distributed across mammals (84, 85), such as those hijacked for the biogenesis of ROs. ROs are common for all positive-sense RNA viruses. They are membranous structures that serve as platforms for the assembly of the virus RTC (43, 85). In the case of coronaviruses, ROs take the form of DMVs, which, besides aiding in genome replication and transcription, also conceal intermediate products of RNA synthesis (i.e., dsRNA) away from innate sensors (12, 14, 86). Therefore, ROs represent critical structures for coronavirus replication. Because the formation of ROs needs to occur before the replication of the virus genome (11, 31, 48), an emerging coronavirus that is adapting to a new host should be able to utilize the cellular machinery to create ROs. Otherwise, the virus polymerase cannot synthesize new genome copies and simultaneously introduce mutations that would further aid in the adaptation to the new species. Following this rationale, we hypothesized that SARS-CoV-2 uses a conserved cellular process to build ROs, and that the use of such common pathway

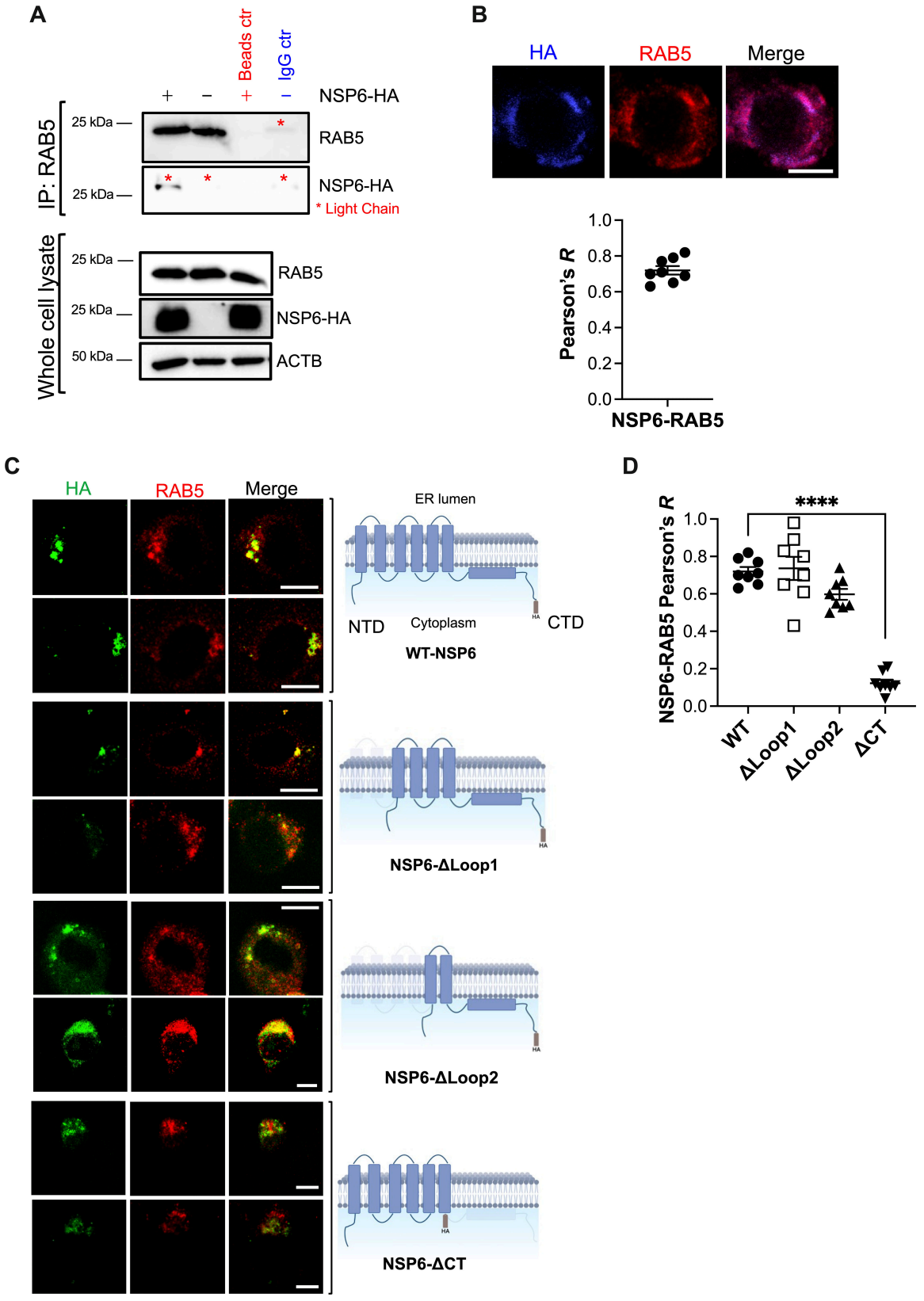

FIG 8 NSP6 interacts and co-localizes with RAB5. (A) HEK293T cells were co-transfected with NSP3, NSP4, and either NSP6-HA or an empty vector. Forty-eight hours later, cells were harvested, and RAB5 was immunoprecipitated. The pulldown fraction was examined for RAB5 and NSP6-HA. Lysates were also analyzed by western blot for RAB5, NSP6-HA, and ACTB. Blots are representative of three independent experiments. (B) VeroE6 cells were co-transfected with NSP6-HA, (Continued on next page)

Fig 8 (Continued)

NSP3, and NSP4. Forty-eight hours later, cells were analyzed by fluorescence microscopy for the distribution of NSP6 relative to RAB5. Images are representative of three independent experiments. Graph: the Pearson's correlation coefficient (*R*) value for the co-localization of RAB5 and NSP6 was calculated from eight randomly selected fields. Individual values, their mean, and SEM are shown. (C) VeroE6 cells were co-transfected with NSP3, NSP4, and either wild-type NSP6-HA or different truncation mutants of NSP6. Forty-eight hours post-transfection, cells were fixed, blocked, and stained for HA and RAB5 to assess their degree of co-localization. Images are representative of three independent experiments. White scale bar: 10 µm. Illustrations of NSP6 mutants were created with BioRender. (D) The Pearson's correlation coefficient (*R*) value for the co-localization of RAB5 and the NSP6 constructs was calculated from eight randomly selected fields. Individual values, their mean, and SEM are represented. ****, $P < 0.0001$.

enabled its transmission across hosts. Uncovering the underlying mechanism by which SARS-CoV-2 creates ROs not only will increase our understanding of the biology of this virus, but also can reveal new targets to treat COVID-19 as well as uncover dependency factors common to other coronaviruses.

Autophagy is an evolutionarily conserved pathway (87) that has been extensively studied for its potential role in RO biogenesis (27), since the DMVs generated during coronavirus infections structurally resemble autophagosomes. In fact, those studies revealed that some coronaviruses usurp autophagic membranes to build ROs (23–30, 88, 89). However, recent reports have shown that autophagy is unnecessary for the assembly of the SARS-CoV-2 RTC (10, 30). Consistent with these findings, no overlap between autophagosome, phagophore, omegasome, or EDEMosome markers and the virus RTC was observed during SARS-CoV-2 RNA replication. Furthermore, deletion of *ATG5*, a gene essential for the formation of autophagosomes (54–57), had no effect on SARS-CoV-2 RNA synthesis. A role for autophagic elements was further excluded by using drugs that modulate this pathway. None of the compounds tested impacted virus genome replication. Only at very high concentrations, the class III PI3K inhibitors 3-MA and VPS34IN downregulated virus RNA. However, we cannot conclude that inhibition of class III PI3K through its role in autophagy accounts for the reduction of SARS-CoV-2 RNA synthesis, since this kinase has pleiotropic effects on other pathways, such as early endosome to late endosome transport, endocytosis, and phosphatidylinositol biosynthetic processes (90–92). Thus, our results are in line with a growing body of evidence that indicates that autophagy is dispensable for the assembly of the SARS-CoV-2 RTC (10, 30).

With the goal of identifying the membranes where SARS-CoV-2 assembles ROs, we examined the subcellular distribution of the virus RTC relative to intracellular membrane markers. Our assays revealed that the virus replication machinery highly overlaps with early endosomes, although some degree of co-localization was also found with Golgi, lipid droplets, and mitochondria. SARS-CoV-2 has been reported to cause extensive disorganization of the Golgi apparatus. In fact, we observed changes in the Golgi in infected cells. However, rather than contributing to the formation of ROs, Golgi fragmentation has been found to provide lipids for RO elongation and facilitate virion trafficking (59, 93). The role of lipid droplets in SARS-CoV-2 infection has recently been explained as a result of the vast membrane rewiring and metabolic reprogramming observed in infected cells (10, 94–96). Similarly, the observation that the SARS-CoV-2 RTC is in close proximity to mitochondria is not novel (97–99), and suggests that the virus positions ROs close to organelles that supply energy and metabolites for the formation and enlargement of its replication factories (31, 100). Despite the partial overlap with Golgi, lipid droplets, and mitochondria, we focused on investigating the role of RAB5 and early endosomes in the replication of the SARS-CoV-2 genome because RAB5 is the marker that most strongly and consistently co-localized with the virus replication machinery. Importantly, RAB5 has already been recognized as an important host dependency factor for SARS-CoV-2 entry (101, 102). SARS-CoV-2 can enter target cells by fusion at the plasma membrane or at endosomal membranes, and this is dependent upon the presence of TMPRSS2 on the cell surface. However, mutations accumulated in the Spike of SARS-CoV-2 variants have resulted in strains that favor fusion at endosomal membranes (65–68). For these strains, RAB5 is an essential factor (102). Because here we

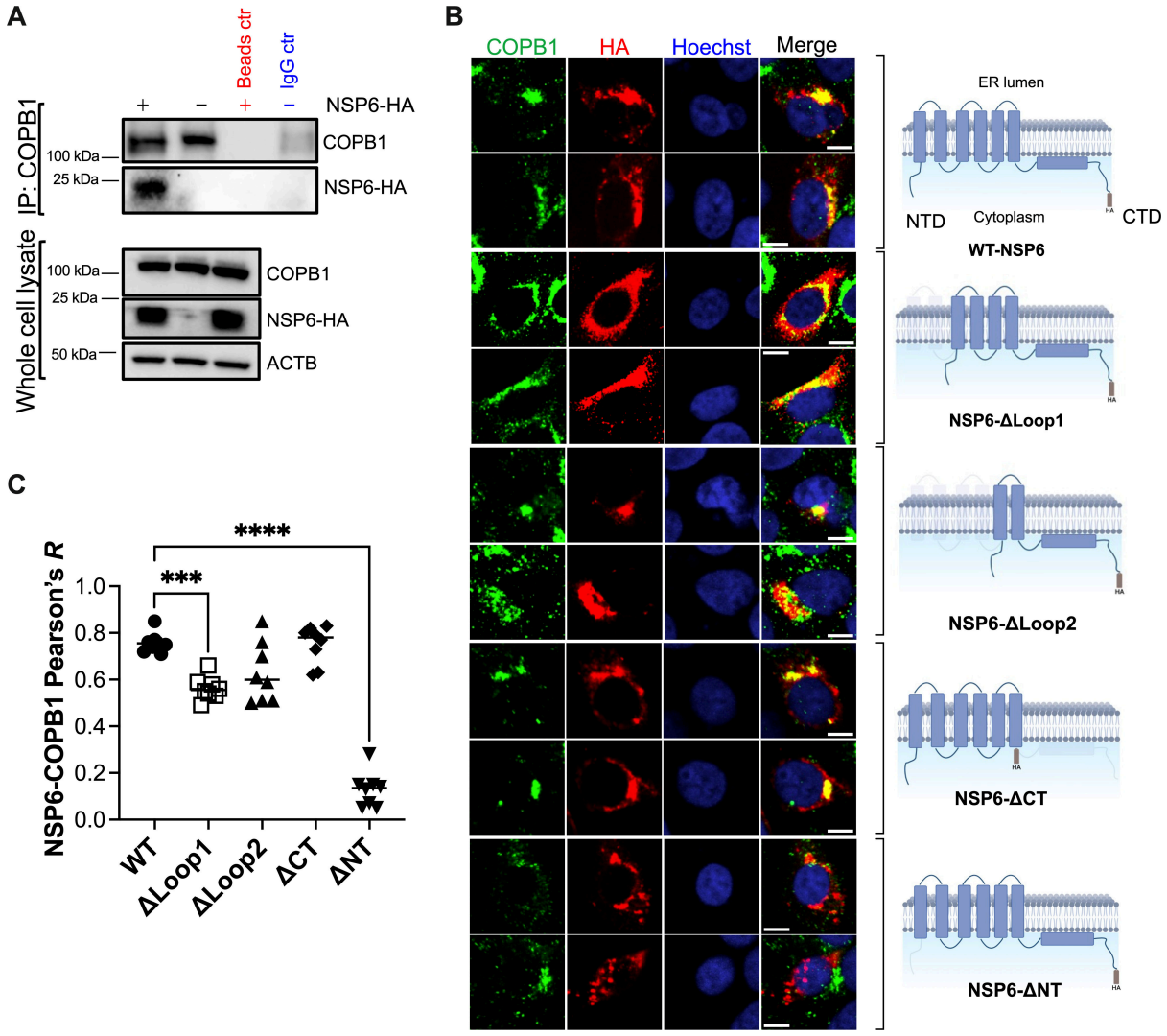

FIG 9 NSP6 interacts and co-localizes with COPB1. (A) HEK293T cells were co-transfected with NSP3, NSP4, and either NSP6-HA or an empty vector. Forty-eight hours later, cells were harvested, and COPB1 was immunoprecipitated. The pulldown fraction was examined for COPB1 and NSP6-HA. Lysates were also analyzed by western blot for COPB1, NSP6-HA, and ACTB. Blots are representative of three independent experiments. (B) VeroE6 cells were co-transfected with NSP3, NSP4, and either wild-type NSP6-HA or different truncation mutants of NSP6. Forty-eight hours post-transfection, cells were fixed, blocked, and stained for COPB1 and HA to assess their degree of overlap. Hoechst was included to label the nucleus. White scale bar: 10 µm. Images are representative of three independent experiments. (C) The Pearson's correlation coefficient (*R*) value for the co-localization of COPB1 and the NSP6 constructs was calculated from eight randomly selected fields. Individual values, their mean, and SEM are represented. Illustrations of NSP6 mutants were created with BioRender. ***, $P < 0.001$; ****, $P < 0.0001$.

used a strain that relies on TMPRSS2 for entry, we were able to identify another critical role of RAB5 in SARS-CoV-2 replication.

Our studies demonstrate that RAB5 is crucial to build ROs. This may be explained by two scenarios: either the virus repositions RAB5 to RO membranes or the virus uses early endosomes (RAB5$^+$ membranes) to generate ROs. To discriminate between these two possibilities, we used the endosomal inhibitors pitstop2, a clathrin inhibitor, and dynasore, a dynamin inhibitor, and examined their impact on SARS-CoV-2 genome replication. Clathrin is fundamental for the maintenance of the cellular early endosomal population by constant vesicular transport from the plasma membrane and other organelles, where Golgi is critical in this process (63, 64). However, dynamins only participate in endosome formation from the plasma membrane (103). Our assays revealed that SARS-CoV-2 needs clathrin to facilitate virus genome replication, while

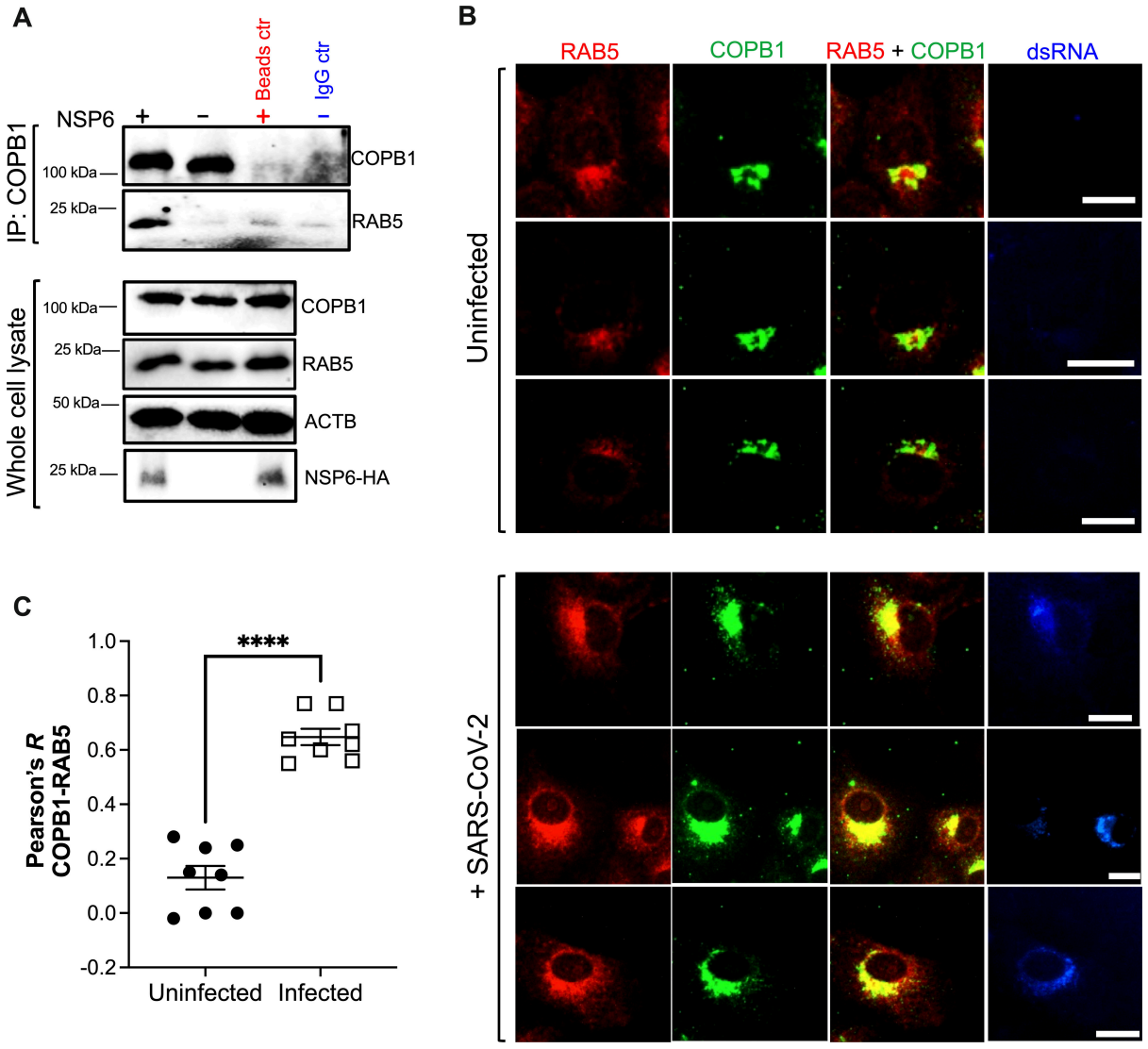

FIG 10 NSP6 enhances an association between RAB5 and COPB1. (A) HEK293T cells were co-transfected with NSP3, NSP4, and either NSP6-HA or an empty vector. Forty-eight hours later, cells were harvested, and COPB1 was immunoprecipitated. The pulldown fraction was examined for COPB1 and RAB5. Lysates were also analyzed by western blot for COPB1, NSP6-HA, RAB5, and ACTB. Blots are representative of three independent experiments. (B) VeroE6 cells were infected with SARS-CoV-2 HK (MOI = 1). Uninfected cells were included as control. Six hours later, cells were stained for RAB5 (red) and COPB1 (green). dsRNA (blue) was included to stain for infected cells. White scale bar: 10 µm. Images are representative of three independent experiments. (C) The Pearson's correlation coefficient (*R*) value for the co-localization of COPB1 and RAB5 was calculated from eight randomly selected fields. Individual values, their mean, and SEM are represented. ****, $P < 0.0001$.

dynamins play a secondary role. Hence, these findings suggest that SARS-CoV-2 needs early endosomes (not just RAB5) for RNA synthesis, and that endocytic vesicles are not the primary source.

The requirement of RAB5$^+$ endosomes for SARS-CoV-2 genome replication was confirmed in *RAB5* knockout cells, where (i) virus RNA synthesis was severely inhibited, (ii) the virus RTC was almost undetectable by fluorescence microscopy, and (iii) only few ROs were visible by electron microscopy. To understand how SARS-CoV-2 repurposes RAB5$^+$ membranes for RO biogenesis, we studied the role of NSP6, since this protein is essential for the reorganization of DMVs to create functional ROs (9, 15, 104–107). In fact, a role for NSP6 in SARS-CoV-2 genome replication was confirmed using K22 (10, 15), an NSP6-specific inhibitor, which significantly reduced virus RNA synthesis. Our data confirmed that NSP6 co-localizes with the virus RTC. Furthermore, NSP6 and the RTC

co-purify with the early endosomal fraction. This subcellular distribution likely explains NSP6 co-immunoprecipitation with the RdRp. However, whether this is a stable or a transient interaction is currently unknown. Our findings also suggest that NSP6 uses its C-terminal domain to interact with RAB5.

NSP6 is a multipass transmembrane protein found in the ER (104, 108, 109), away from endosomal membranes. So, how can this protein recruit early endosomes from the ER to generate ROs? A possible answer may be found in the fact that the endocytic pathway plays an important role in ER architecture and structure (110). Contact sites between the ER and endosomes have been reported to enable inter-organelle communication in a vesicular-independent manner and facilitate the exchange of lipids and small molecules (111–114). In addition to this molecular trade, membrane contacts between ER and endosomes are important for endosome fission, positioning, calcium exchange, and dephosphorylation of endosomal receptors (111, 115–122). In fact, it is estimated that 50% of early endosomes are in contact with the ER, and COP-I, a component of the retrograde transport from the Golgi apparatus to the ER, plays an important role in connecting endosomes to the ER (38, 39). Remarkably, we found that COPB1, which is part of the COP-I complex, is required to support SARS-CoV-2 genome replication, and previous studies with SARS-CoV-1 already identified COPB1 as a cellular factor that contributes to RO biogenesis (123–125). Therefore, it is likely that ER-bound NSP6 recruits endosomal membranes at these contact sites in a COP-I-dependent manner, and this is consistent with our *COPB1*KO assays, in which virus RNA synthesis is severely inhibited, and our immunoprecipitation and imaging studies showing not only NSP6-COPB1 and NSP6-RAB5 interactions, but also that NSP6 enhances an association between RAB5 and COPB1. Unlike its co-localization with RAB5, NSP6 co-localization with COPB1 requires the NSP6 N-terminus, which would theoretically allow NSP6 to interact with both molecules simultaneously. However, whether this interaction is direct and if the same NSP6 molecule is interacting with both COPB1 and RAB5 remains unclear.

Whereas the connection between the ER and early endosomes, and the implication of COPB1 in this process, helps understand how SARS-CoV-2 repurposes these membranes to create ROs, two questions remain unanswered: first, why does the virus use membranes from early endosomes instead of other endosomal structures? Second, does SARS-CoV-2 co-opt highly conserved cellular factors for RO biogenesis? For the first question, we could speculate that exploitation of early endosomes to create ROs allows for evasion of innate sensors. While endosomal Toll-like receptors (TLRs) are present in all endosomal membranes, for the most part, these pattern recognition receptors require pH-dependent proteolytic activation. Hence, by using membranes where TLR3 and TLR7/8 are less active, the virus genome, subgenomic RNAs, and dsRNA intermediates are less susceptible to being recognized by the innate sensing system (126–128) —offering the virus an advantage when parasitizing the cell. As for the second question, autophagy seemed a perfect candidate due to its evolutionary conservation and the creation of double membrane vesicles (autophagosomes). However, our findings indicate the endosomal pathway is critical for virus genome replication. Still, like autophagy, endocytosis and vesicular trafficking are widely distributed in metazoans with many components sharing a high degree of conservation within mammals (40). For instance, the clathrin heavy chain shares 100% identity within primates and 90% identity with rodents. Similarly, RAB5A shares 90% identity with that of canids, cattle, and rodents. COPB1 has 94% similarity with canids and bovine, and over 98% similarity with other primates. Hence, this high conservation, along with a potential selective advantage of using membranes with less active innate sensors, may have allowed SARS-CoV-2 to find an appropriate environment to support its replication in different mammalian species, which ultimately might have facilitated its propagation and adaptation to new hosts.

MATERIALS AND METHODS

For detailed methods, refer to the supplemental material.

Plasmids

Plasmids coding SARS-CoV-2 open reading frames (ORFs) were gifts from Dr. Konstantin Sparrer. HA-tagged full-length and truncated *NSP6* constructs were cloned into pcDNA5 (ThermoFisher Scientific, V601020). *ATG5*^{KO} cells were engineered using LentiCRISPRv2-*ATG5* (Addgene plasmid # 99573) (129). *COPB1*^{KO} and *RAB5*^{KO} cells were generated by transduction of LentiCRISPRv2 (Addgene plasmid # 52961) (130) harboring the following sgRNAs: *COPB1*: 5′-CAGGTTATCAAAGCGCTGAA-3′ and 5′-AGGTAGCACAAAACGAATGA-3′; *RAB5*: 5′-CGAGGCGCAACAAGACCCAA-3′ and 5′-GAGGCGCAACAAGACCCAAC-3′. psPAX2 (Addgene plasmid # 12260) and p-MD2-G (Addgene plasmid # 12259) were used to generate lentiviral particles to deliver Cas9 and sgRNAs, as well as to generate stable cell lines, following our previously reported protocols (131, 132). EGFP-LC3B was cloned into pQCXIP. pMX-EGFP-FYVE1 (Addgene plasmid # 38269) (133) was used to express DFCP1/FYVE1. Addgene plasmid # 80351 was used to express the dominant-negative mutant of VPS4, VPS4$_{E228Q}$-EGFP (134). The Addgene plasmid # 14437 was used to express RAB5A fused with RFP (135).

Cell culture and transfections

All cells were cultured in complete medium and supplemented with appropriate antibiotics and growth factors, following the manufacturer's instructions as well as our previously established protocols (131, 132, 136). Cells were transfected using GenJet *in vitro* DNA transfection reagent (SignaGen Laboratories, SL100488) or Lipofectamine 3000 Transfection Reagent (ThermoFisher Scientific, L3000001), following the manufacturers' instructions.

Knockdown assays

esiRNA oligos were obtained to deplete *AP1*, *AP2*, and *COPB1* (ThermoFisher Scientific #138604, #14075, #s3373, respectively). A control siRNA SignalSilence was used (ThermoFisher Scientific, #6568). Knockdown of target genes was achieved by transient transfection of the esiRNAs in 10^6 HEK293T-ACE2 cells using Lipofectamine 3000, following the manufacturer's instructions. Knockdown was verified by western blot.

XTT assay

XTT assays were performed in 2×10^4-infected and uninfected VeroE6 cells in the presence of DMSO, 3-MA, VPS34IN, K22, or pitstop2, following our previously established protocol (137).

SARS-CoV-2 infections

All infections were performed at the URMC Biosafety Level 3 (BSL3) laboratory, following the approved standard operating procedures.

Cells were infected with SARS-CoV-2 isolate Hong Kong (BEI Resources, NR52282; GenBank: MT547814) at MOI = 1, unless noted differently. Infections were kept at 4°C for 1 h for synchronization. Infected cells were maintained and processed as previously described (132). For RNA kinetics assays, cells were harvested at 2, 4, 6, 8, 10, 16, 24, and 48 h post-infection. In parallel, supernatants were collected for $TCID_{50}$ assays. Similar infections were performed in the presence of siRNAs, cells depleted from ATG5, RAB5, or COPB1, or in the presence of drugs targeting autophagy, endocytosis, Golgi transport, or NSP6.

Luciferase reporter assay

One million parental, *RAB5*KO, and/or *COPB1*KO HEK293T-ACE2-30F-PLP2 cells were infected with SARS-CoV-2 HK at MOIs 2 and 5. Four hours later, cells were harvested,

and firefly and renilla luciferase activities were measured by luminescence using a microplate reader (BMG LABTECH, LUMIstar Omega). Uninfected cells were included for both parental and KO cells to subtract any background firefly luminescence. Data are presented as firefly luciferase over renilla luciferase.

RT-qPCR

RNA extraction and cDNA synthesis were performed following our previously established protocol (131, 132, 137, 138). cDNA was used to measure the levels of SARS-CoV-2 RNA by qPCR using primers for NSP12 and NSP6, following our established qPCR method, including primers for quality control (131, 132, 137, 138). Changes in *NSP12* and *NSP6* RNA levels were determined by the $2^{\Delta\Delta Cq}$ method using *GAPDH* as the housekeeping gene. SARS-CoV-2 genome replication was calculated as fold-change over basal viral RNA. A fold-change of >2.0 or <0.5 relative to the control samples was considered biologically relevant (58).

Median $TCID_{50}$ assay

SARS-CoV-2 virus stocks and culture supernatants from infections were titrated by measuring their cytopathic effect by optical microscopy 3 days post-infection using the Spearman-Kärber method (139).

Immunoprecipitation and western blotting

Infected, uninfected, and transfected cells were processed for immunoprecipitation and/or western blot following our previously established protocols, including handling of BSL3 samples (131, 132). Target proteins were pulled down using the primary antibodies listed in Table 1. Similarly, western blot membranes were probed with the primary and secondary antibodies listed in Table 1.

Endosomal fractionation assay

HEK293T cells expressing SARS-CoV-2 NSP3, NSP4, NSP6-HA, and streptavidin-tagged RdRp (NSP12) were harvested, washed on ice-cold Dulbecco's phosphate buffered saline (DPBS), and lysed to obtain early endosomal and cytosolic fractions, following the Trident Endosome Isolation kit and instructions (GenTex, GTX35192). Whole cell lysate, cytosolic, and early endosomal fractions were analyzed by western blot for the presence of NSP6 (HA), RdRp (Strep), and the GST control (HA). Purity of the fractions was confirmed using antibodies against early endosomal markers (RAB5, EEA1), late endosomal markers (RAB7), cytosolic markers (non-prenylated RAB5), plasma membrane markers (Na/K ATPase), ER markers (calnexin), and cytoskeleton markers (ACTB) (see Table 1 for antibody specifications).

Fluorescence microscopy

Infected, uninfected, and transfected cells were washed with DPBS, permeabilized, and fixed following our previously established protocol, including handling of BSL3 samples (132). Target proteins were visualized using antibodies listed in Table 1. The nuclei were stained with Hoechst (ThermoFisher Scientific, H3570; 1:5,000 dilution). Slides were imaged in a BioTek Lionheart FX automated microscope and a Nikon A1R HD with TIRF confocal microscope using 40× and 60×/1.49 oil objectives, respectively, and filter cubes/excitation diodes 350 nm, 488 nm, and 586 nm in order to excite 4',6-diamidino-2-phenylindole (DAPI), EGFP, and TexasRed, respectively. Images were processed and analyzed using the Gen5 software (BioTek Instruments, Winooski, VT). Proportional adjustments of brightness/contrast were applied.

TABLE 1 Antibody sources and conditions

Protein	Primary antibody	Dilution	Source
ACTB/β-actin	Mouse monoclonal (8H10D10C4) to ACTB/β-actin	1:1,000	Cell Signaling Technology, 3700S
ADRP	Mouse monoclonal (2 C5A3) to ADRP	1:100	ThermoFisher Scientific, MA5-24797
ATG5	Rabbit polyclonal to ATG5	1:1,000	Cell Signaling Technology, 2630S
Calnexin	Mouse monoclonal (AF18) to CALNEXIN	1:100	ThermoFisher Scientific, MA3-027
CD63	Mouse monoclonal (MEM-259) to CD63 (LAMP-3)	1:100	ThermoFisher Scientific, MA1-19281
CD81	Mouse monoclonal (1.3.3.22) to CD81	1:100	ThermoFisher Scientific, MA5-13548
COPB1	Rabbit polyclonal to beta COP	1:1,000 1:100 for IP	ThermoFisher Scientific, PA1-061
dsRNA	Mouse monoclonal (rJ2) to dsRNA	1:200	Sigma-Aldrich, MABE1134
EDEM1	Rabbit polyclonal to EDEM1	1:100	Sigma-Aldrich, HPA029565
EEA1	Rabbit polyclonal to EEA1	1:1,000	Cell Signaling Technology, 2411
Flag	Rabbit monoclonal to DYKDDDDK	1:100	Cell Signaling Technology, 14793
GFP	Mouse monoclonal (4B10B2) to GFP	1:1,000	Sigma-Aldrich, SAB5300167
GOSR1	Mouse monoclonal (HFD9-5) to GOSR1	1:100	ThermoFisher Scientific, MA1-91008
HA	Mouse monoclonal to HA	1:1,000 for WB, 1:100 for flow cytometry, IP and microscopy	Biolegend, 901502
LC3B	Rabbit polyclonal to LC3B	1:1,000	Cell Signaling Technology, 2775S
	Rabbit monoclonal (D11) to LC3B	1:100	Cell Signaling Technology, 3868
Mouse IgG	Goat anti-mouse (H + L) secondary HRP	1:2,000	ThermoFisher Scientific, 31430
Mouse IgG_1	Rat anti-mouse IgG1 APC conjugated	1:100	ThermoFisher Scientific, 17–4015-82
Mouse IgG_1	Goat polyclonal (Alexa-488 conjugated)	1:500	ThermoFisher Scientific, A-21121
Mouse IgG_1	Goat polyclonal (Alexa-568 conjugated)	1:500	ThermoFisher Scientific, A-21124
Mouse IgG_{2a}	Goat anti-mouse IgG_{2a} (Alexa-350 conjugated)	1:500	ThermoFisher Scientific, A-21130
Mouse IgG_{2a}	Goat polyclonal (Alexa-488 conjugated)	1:500	ThermoFisher Scientific, A-21131
Mouse IgG_{2a}	Goat polyclonal (Alexa-568 conjugated)	1:500	ThermoFisher Scientific, A-21134
Na/K ATPase	Rabbit polyclonal	1:1,000	Cell Signaling Technology, 3010
RAB11	Mouse monoclonal (1A12B9D8) to RAB11	1:100	ThermoFisher Scientific, MA5-31876

(*Continued on next page*)

TABLE 1 Antibody sources and conditions (*Continued*)

Protein	Primary antibody	Dilution	Source
RAB5A	Mouse monoclonal (E6N8S) to RAB5A	1:1,000 for WB, 1:100 for microscopy and IP	Cell Signaling Technology, 46449
RAB7A	Rabbit polyclonal to RAB7A	1:1,000	Abcam, ab77993
Rabbit IgG	Goat anti-rabbit IgG (H + L), HRP conjugated	1:4,000	Promega, W4011
Rabbit IgG	Goat anti-Rabbit IgG (H + L) PE-Cy5.5	1:500	ThermoFisher Scientific, L42018
Rabbit IgG	Goat polyclonal (Alexa-488 conjugated)	1:500	ThermoFisher Scientific, A-11008
Rabbit IgG	Goat polyclonal (Alexa-568 conjugated)	1:500	ThermoFisher Scientific, A-11011
SARS-CoV-2 N	Rabbit monoclonal (ARC2372) to SARS-CoV-2 nucleoprotein	1:1,000	ThermoFisher Scientific, MA5-36086
SARS-CoV-2 NSP6	Rabbit polyclonal to SARS-CoV2-NSP6	1:100	ProSci, 9177
SARS-CoV-2 NSP12	Rabbit polyclonal to SARS-CoV-2 NSP12	1:100	GeneTex, GTX135467
SQSTM1/p62	Rabbit monoclonal (D1Q5S) to SQSTM1/p62	1:100	Cell Signaling Technology, 39749
Strep	Rabbit polyclonal to Strep-tag-II	1:1,000	Abcam, ab76949
TGN46	Mouse monoclonal (2 F7.1) to TGN46	1:100	ThermoFisher Scientific, MA3-063
WIPI2	Rabbit polyclonal to WIPI2	1:100	Abcam, ab229225

Electron microscopy

Parental and *RAB5*KO VeroE6 cells were infected with SARS-CoV-2 HK at an MOI = 5. As controls, uninfected parental and *RAB5*KO cells were included. Six hours later, cells were fixed in 2.5% glutaraldehyde and 4% paraformaldehyde in 0.1 M sodium cacodylate buffer and incubated for 24 h at 4°C. Next, cells were processed in the electron microscopy facility for thin sectioning at 70 nm. The sections were placed onto formvar/carbon copper slot grids and stained with aqueous uranyl acetate and 0.3% lead citrate. The grids were imaged using a Hitachi 7650 transmission electron microscope and an AMT 12 MP NanoSprint12 digital camera.

Statistical analysis

Statistical calculations for two-group comparisons were performed with a two-tailed unpaired Student's *t*-test. All other statistical comparisons were performed with one-way analysis of variance with Dunnett's *post hoc* testing. Analyses were performed using Graph Pad Prism version 10.3.0. *P*-values ≤0.05 were considered statistically significant.

ACKNOWLEDGMENTS

We thank Dr. Yuhang Shi (Chinese Academy of Medical Sciences and Beijing Union Medical College, Beijing, China) for technical support in this project. We thank Dr. Joshua Munger (University of Rochester Medical Center) for providing the MRC5-ACE2 cells. We are grateful to the Center for Advanced Research Technologies (CART) at the University of Rochester, especially Drs. Martin Pavelka and Sonia Rosenberger for training us to use the URMC BSL3 facility, as well as Karen Bentley, Dr. Chad Galloway, and Kelsea Cristillo at the Electron Microscopy core for processing samples by TEM.

This work has been supported by the National Science Foundation (NSF RAPID MCB-2032518; Ruth Serra-Moreno, PI) and the University of Rochester (Ruth

Serra-Moreno, startup funds). Konstantin Sparrer was supported by the German Research Society (DFG; SPP1923, RC1279, SP 1600/7-1, SP 1600/9-1) and the German Federal Ministry for Education and Research (BMBF, project IMMUNOMOD 01KI2014).

AUTHOR AFFILIATIONS

[1]Microbiology and Immunology, University of Rochester Medical Center, Rochester, New York, USA
[2]Institute of Molecular Virology, Ulm University Medical Center, Ulm, Germany
[3]German Center for Neurodegenerative Diseases (DZNE), Ulm, Germany

AUTHOR ORCIDs

Ruth Serra-Moreno http://orcid.org/0000-0002-1923-6414

FUNDING

Funder	Grant(s)	Author(s)
National Science Foundation	MCB-2032518	Yuexuan Chen Ruth Serra-Moreno
UR | University of Rochester Medical Center (URMC)	OP211970	Yuexuan Chen Ruth Serra-Moreno
Deutsche Forschungsgemeinschaft	SPP1923,RC1279,SP 1600/7-1,SP 1600/9-1	Konstantin Maria Johannes Sparrer
Bundesministerium für Bildung und Forschung	IMMUNOMOD 01KI2014	Konstantin Maria Johannes Sparrer

AUTHOR CONTRIBUTIONS

Yuexuan Chen, Conceptualization, Data curation, Formal analysis, Investigation, Methodology, Writing – review and editing | Susanne Klute, Conceptualization, Formal analysis, Investigation, Methodology | Konstantin Maria Johannes Sparrer, Conceptualization, Formal analysis, Resources, Writing – review and editing | Ruth Serra-Moreno, Conceptualization, Formal analysis, Funding acquisition, Project administration, Resources, Supervision, Writing – original draft, Writing – review and editing

DATA AVAILABILITY

All relevant data are in the article and its supplemental material. All reagents generated in this study are available from the lead contact upon request.

ADDITIONAL FILES

The following material is available online.

Supplemental Material

Supplemental material (mBio03314-24-s0001.pdf). Extended methods and supplemental figures.

REFERENCES

1. Dhama K, Patel SK, Sharun K, Pathak M, Tiwari R, Yatoo MI, Malik YS, Sah R, Rabaan AA, Panwar PK, Singh KP, Michalak I, Chaicumpa W, Martinez-Pulgarin DF, Bonilla-Aldana DK, Rodriguez-Morales AJ. 2020. SARS-CoV-2 jumping the species barrier: zoonotic lessons from SARS, MERS and recent advances to combat this pandemic virus. Travel Med Infect Dis 37:101830. https://doi.org/10.1016/j.tmaid.2020.101830
2. Ruiz-Aravena M, McKee C, Gamble A, Lunn T, Morris A, Snedden CE, Yinda CK, Port JR, Buchholz DW, Yeo YY, et al. 2022. Ecology, evolution and spillover of coronaviruses from bats. Nat Rev Microbiol 20:299–314. https://doi.org/10.1038/s41579-021-00652-2
3. Latinne A, Hu B, Olival KJ, Zhu G, Zhang L, Li H, Chmura AA, Field HE, Zambrana-Torrelio C, Epstein JH, Li B, Zhang W, Wang LF, Shi ZL, Daszak P. 2020. Origin and cross-species transmission of bat coronaviruses in China. Nat Commun 11:4235. https://doi.org/10.1038/s41467-020-17687-3

4. Hu B, Ge X, Wang LF, Shi Z. 2015. Bat origin of human coronaviruses. Virol J 12:221. https://doi.org/10.1186/s12985-015-0422-1
5. Lawler OK, Allan HL, Baxter PWJ, Castagnino R, Tor MC, Dann LE, Hungerford J, Karmacharya D, Lloyd TJ, López-Jara MJ, Massie GN, Novera J, Rogers AM, Kark S. 2021. The COVID-19 pandemic is intricately linked to biodiversity loss and ecosystem health. Lancet Planet Health 5:e840–e850. https://doi.org/10.1016/S2542-5196(21)00258-8
6. Louz D, Bergmans HE, Loos BP, Hoeben RC. 2005. Cross-species transfer of viruses: implications for the use of viral vectors in biomedical research, gene therapy and as live-virus vaccines. J Gene Med 7:1263–1274. https://doi.org/10.1002/jgm.794
7. Kalvatchev N, Sirakov I. 2021. Respiratory viruses crossing the species barrier and emergence of new human coronavirus infectious disease. Biotech Biotechnol Equip 35:37–42. https://doi.org/10.1080/13102818.2020.1843539
8. Webby R, Hoffmann E, Webster R. 2004. Molecular constraints to interspecies transmission of viral pathogens. Nat Med 10:S77–S81. https://doi.org/10.1038/nm1151
9. Angelini MM, Akhlaghpour M, Neuman BW, Buchmeier MJ. 2013. Severe acute respiratory syndrome coronavirus nonstructural proteins 3, 4, and 6 induce double-membrane vesicles. mBio 4:e00524-13. https://doi.org/10.1128/mBio.00524-13
10. Ricciardi S, Guarino AM, Giaquinto L, Polishchuk EV, Santoro M, Di Tullio G, Wilson C, Panariello F, Soares VC, Dias SSG, Santos JC, Souza TML, Fusco G, Viscardi M, Brandi S, Bozza PT, Polishchuk RS, Venditti R, De Matteis MA. 2022. The role of NSP6 in the biogenesis of the SARS-CoV-2 replication organelle. Nature 606:761–768. https://doi.org/10.1038/s41586-022-04835-6
11. Snijder EJ, Limpens RWAL, de Wilde AH, de Jong AWM, Zevenhoven-Dobbe JC, Maier HJ, Faas FFGA, Koster AJ, Bárcena M. 2020. A unifying structural and functional model of the coronavirus replication organelle: tracking down RNA synthesis. PLoS Biol 18:e3000715. https://doi.org/10.1371/journal.pbio.3000715
12. Wolff G, Melia CE, Snijder EJ, Bárcena M. 2020. Double-membrane vesicles as platforms for viral replication. Trends Microbiol 28:1022–1033. https://doi.org/10.1016/j.tim.2020.05.009
13. Oudshoorn D, Rijs K, Limpens RWAL, Groen K, Koster AJ, Snijder EJ, Kikkert M, Bárcena M. 2017. Expression and cleavage of Middle east respiratory syndrome coronavirus nsp3-4 polyprotein induce the formation of double-membrane vesicles that mimic those associated with coronaviral RNA replication. mBio 8:e01658-17. https://doi.org/10.1128/mBio.01658-17
14. Roingeard P, Eymieux S, Burlaud-Gaillard J, Hourioux C, Patient R, Blanchard E. 2022. The double-membrane vesicle (DMV): a virus-induced organelle dedicated to the replication of SARS-CoV-2 and other positive-sense single-stranded RNA viruses. Cell Mol Life Sci 79:425. https://doi.org/10.1007/s00018-022-04469-x
15. Lundin A, Dijkman R, Bergström T, Kann N, Adamiak B, Hannoun C, Kindler E, Jónsdóttir HR, Muth D, Kint J, Forlenza M, Müller MA, Drosten C, Thiel V, Trybala E. 2014. Targeting membrane-bound viral RNA synthesis reveals potent inhibition of diverse coronaviruses including the Middle East respiratory syndrome virus. PLoS Pathog 10:e1004166. https://doi.org/10.1371/journal.ppat.1004166
16. Bills C, Xie X, Shi PY. 2023. The multiple roles of nsp6 in the molecular pathogenesis of SARS-CoV-2. Antiviral Res 213:105590. https://doi.org/10.1016/j.antiviral.2023.105590
17. Bills CJ, Xia H, Chen JY-C, Yeung J, Kalveram BK, Walker D, Xie X, Shi P-Y. 2023. Mutations in SARS-CoV-2 variant nsp6 enhance type-I interferon antagonism. Emerg Microbes Infect 12:2209208. https://doi.org/10.1080/22221751.2023.2209208
18. Miller S, Krijnse-Locker J. 2008. Modification of intracellular membrane structures for virus replication. Nat Rev Microbiol 6:363–374. https://doi.org/10.1038/nrmicro1890
19. Magliano D, Marshall JA, Bowden DS, Vardaxis N, Meanger J, Lee JY. 1998. Rubella virus replication complexes are virus-modified lysosomes. Virology (Auckl) 240:57–63. https://doi.org/10.1006/viro.1997.8906
20. Miller DJ, Schwartz MD, Ahlquist P. 2001. Flock house virus RNA replicates on outer mitochondrial membranes in *Drosophila* cells. J Virol 75:11664–11676. https://doi.org/10.1128/JVI.75.23.11664-11676.2001
21. Snijder EJ, van der Meer Y, Zevenhoven-Dobbe J, Onderwater JJM, van der Meulen J, Koerten HK, Mommaas AM. 2006. Ultrastructure and origin of membrane vesicles associated with the severe acute respiratory syndrome coronavirus replication complex. J Virol 80:5927–5940. https://doi.org/10.1128/JVI.02501-05
22. Stertz S, Reichelt M, Spiegel M, Kuri T, Martínez-Sobrido L, García-Sastre A, Weber F, Kochs G. 2007. The intracellular sites of early replication and budding of SARS-coronavirus. Virology (Auckl) 361:304–315. https://doi.org/10.1016/j.virol.2006.11.027
23. Jackson WT, Giddings TH, Taylor MP, Mulinyawe S, Rabinovitch M, Kopito RR, Kirkegaard K. 2005. Subversion of cellular autophagosomal machinery by RNA viruses. PLoS Biol 3:e156. https://doi.org/10.1371/journal.pbio.0030156
24. Kirkegaard K. 2009. Subversion of the cellular autophagy pathway by viruses. Curr Top Microbiol Immunol 335:323–333. https://doi.org/10.1007/978-3-642-00302-8_16
25. Wileman T. 2006. Aggresomes and autophagy generate sites for virus replication. Science 312:875–878. https://doi.org/10.1126/science.1126766
26. Knoops K, Kikkert M, Worm SHE van den, Zevenhoven-Dobbe JC, van der Meer Y, Koster AJ, Mommaas AM, Snijder EJ. 2008. SARS-coronavirus replication is supported by a reticulovesicular network of modified endoplasmic reticulum. PLoS Biol 6:e226. https://doi.org/10.1371/journal.pbio.0060226
27. Cottam EM, Maier HJ, Manifava M, Vaux LC, Chandra-Schoenfelder P, Gerner W, Britton P, Ktistakis NT, Wileman T. 2011. Coronavirus nsp6 proteins generate autophagosomes from the endoplasmic reticulum via an omegasome intermediate. Autophagy 7:1335–1347. https://doi.org/10.4161/auto.7.11.16642
28. Prentice E, Jerome WG, Yoshimori T, Mizushima N, Denison MR. 2004. Coronavirus replication complex formation utilizes components of cellular autophagy. J Biol Chem 279:10136–10141. https://doi.org/10.1074/jbc.M306124200
29. Reggiori F, Monastyrska I, Verheije MH, Calì T, Ulasli M, Bianchi S, Bernasconi R, de Haan CAM, Molinari M. 2010. Coronaviruses hijack the LC3-I-positive EDEMosomes, ER-derived vesicles exporting short-lived ERAD regulators, for replication. Cell Host Microbe 7:500–508. https://doi.org/10.1016/j.chom.2010.05.013
30. Twu WI, Lee JY, Kim H, Prasad V, Cerikan B, Haselmann U, Tabata K, Bartenschlager R. 2021. Contribution of autophagy machinery factors to HCV and SARS-CoV-2 replication organelle formation. Cell Rep 37:110049. https://doi.org/10.1016/j.celrep.2021.110049
31. Cortese M, Lee J-Y, Cerikan B, Neufeldt CJ, Oorschot VMJ, Köhrer S, Hennies J, Schieber NL, Ronchi P, Mizzon G, et al. 2020. Integrative imaging reveals SARS-CoV-2-induced reshaping of subcellular morphologies. Cell Host Microbe 28:853–866. https://doi.org/10.1016/j.chom.2020.11.003
32. Klatte N, Shields DC, Agoni C. 2022. Modelling the transitioning of SARS-CoV-2 nsp3 and nsp4 lumenal regions towards a more stable state on complex formation. Int J Mol Sci 24:720. https://doi.org/10.3390/ijms24010720
33. Eymieux S, Rouillé Y, Terrier O, Seron K, Blanchard E, Rosa-Calatrava M, Dubuisson J, Belouzard S, Roingeard P. 2021. Ultrastructural modifications induced by SARS-CoV-2 in vero cells: a kinetic analysis of viral factory formation, viral particle morphogenesis and virion release. Cell Mol Life Sci 78:3565–3576. https://doi.org/10.1007/s00018-020-03745-y
34. Woodman PG. 2000. Biogenesis of the sorting endosome: the role of Rab5. Traffic 1:695–701. https://doi.org/10.1034/j.1600-0854.2000.010902.x
35. Olchowik M, Miaczyńska M. 2009. Effectors of GTPase Rab5 in endocytosis and signal transduction. Postepy Biochem 55:171–180.
36. Yuan W, Song C. 2020. The emerging role of Rab5 in membrane receptor trafficking and signaling pathways. Biochem Res Int 2020:4186308. https://doi.org/10.1155/2020/4186308
37. Nielsen E, Severin F, Backer JM, Hyman AA, Zerial M. 1999. Rab5 regulates motility of early endosomes on microtubules. Nat Cell Biol 1:376–382. https://doi.org/10.1038/14075
38. Johannes L, Pezo V, Mallard F, Tenza D, Wiltz A, Saint-Pol A, Helft J, Antony C, Benaroch P. 2003. Effects of HIV-1 Nef on retrograde transport from the plasma membrane to the endoplasmic reticulum. Traffic 4:323–332. https://doi.org/10.1034/j.1600-0854.2003.00089.x
39. Llorente A, Lauvrak SU, van Deurs B, Sandvig K. 2003. Induction of direct endosome to endoplasmic reticulum transport in Chinese hamster ovary (CHO) cells (LdlF) with a temperature-sensitive defect in epsilon-coatomer protein (epsilon-COP). J Biol Chem 278:35850–35855. https://doi.org/10.1074/jbc.M303425200

40. Dergai M, Iershov A, Novokhatska O, Pankivskyi S, Rynditch A. 2016. Evolutionary changes on the way to clathrin-mediated endocytosis in animals. Genome Biol Evol 8:588–606. https://doi.org/10.1093/gbe/evw028
41. Hsu N-Y, Ilnytska O, Belov G, Santiana M, Chen Y-H, Takvorian PM, Pau C, van der Schaar H, Kaushik-Basu N, Balla T, Cameron CE, Ehrenfeld E, van Kuppeveld FJM, Altan-Bonnet N. 2010. Viral reorganization of the secretory pathway generates distinct organelles for RNA replication. Cell 141:799–811. https://doi.org/10.1016/j.cell.2010.03.050
42. Nagy PD, Pogany J. 2011. The dependence of viral RNA replication on co-opted host factors. Nat Rev Microbiol 10:137–149. https://doi.org/10.1038/nrmicro2692
43. Nguyen-Dinh V, Herker E. 2021. Ultrastructural features of membranous replication organelles induced by positive-stranded RNA Viruses. Cells 10:2407. https://doi.org/10.3390/cells10092407
44. Malone B, Urakova N, Snijder EJ, Campbell EA. 2022. Structures and functions of coronavirus replication-transcription complexes and their relevance for SARS-CoV-2 drug design. Nat Rev Mol Cell Biol 23:21–39. https://doi.org/10.1038/s41580-021-00432-z
45. Pathak R, Eliscovich C, Mena I, Cupic A, Rutkowska M, Chandran K, Jangra RK, García-Sastre A, Singer RH, Kalpana GV. 2024. Visualization of early RNA replication kinetics of SARS-CoV-2 by using single molecule RNA-FISH combined with immunofluorescence. Viruses 16:262. https://doi.org/10.3390/v16020262
46. V'kovski P, Kratzel A, Steiner S, Stalder H, Thiel V. 2021. Coronavirus biology and replication: implications for SARS-CoV-2. Nat Rev Microbiol 19:155–170. https://doi.org/10.1038/s41579-020-00468-6
47. Snijder EJ, Decroly E, Ziebuhr J. 2016. The nonstructural proteins directing coronavirus RNA synthesis and processing. Adv Virus Res 96:59–126. https://doi.org/10.1016/bs.aivir.2016.08.008
48. Doyle N, Simpson J, Hawes PC, Maier HJ. 2021. Coronavirus RNA synthesis takes place within membrane-bound sites. Viruses 13:2540. https://doi.org/10.3390/v13122540
49. Tanida I, Ueno T, Kominami E. 2008. LC3 and autophagy. Methods Mol Biol 445:77–88. https://doi.org/10.1007/978-1-59745-157-4_4
50. Axe EL, Walker SA, Manifava M, Chandra P, Roderick HL, Habermann A, Griffiths G, Ktistakis NT. 2008. Autophagosome formation from membrane compartments enriched in phosphatidylinositol 3-phosphate and dynamically connected to the endoplasmic reticulum. J Cell Biol 182:685–701. https://doi.org/10.1083/jcb.200803137
51. Polson HEJ, de Lartigue J, Rigden DJ, Reedijk M, Urbé S, Clague MJ, Tooze SA. 2010. Mammalian Atg18 (WIPI2) localizes to omegasome-anchored phagophores and positively regulates LC3 lipidation. Autophagy 6:506–522. https://doi.org/10.4161/auto.6.4.11863
52. Pugsley HR. 2017. Assessing autophagic flux by measuring LC3, p62, and LAMP1 co-localization using multispectral imaging flow cytometry. J Vis Exp:55637. https://doi.org/10.3791/55637
53. Lamark T, Kirkin V, Dikic I, Johansen T. 2009. NBR1 and p62 as cargo receptors for selective autophagy of ubiquitinated targets. Cell Cycle 8:1986–1990. https://doi.org/10.4161/cc.8.13.8892
54. Sanjuan MA, Dillon CP, Tait SWG, Moshiach S, Dorsey F, Connell S, Komatsu M, Tanaka K, Cleveland JL, Withoff S, Green DR. 2007. Toll-like receptor signalling in macrophages links the autophagy pathway to phagocytosis. Nature 450:1253–1257. https://doi.org/10.1038/nature06421
55. Ye X, Zhou XJ, Zhang H. 2018. Exploring the role of autophagy-related gene 5 (*ATG5*) yields important insights into autophagy in autoimmune/autoinflammatory diseases. Front Immunol 9:2334. https://doi.org/10.3389/fimmu.2018.02334
56. Noda NN, Fujioka Y, Hanada T, Ohsumi Y, Inagaki F. 2013. Structure of the Atg12-Atg5 conjugate reveals a platform for stimulating Atg8-PE conjugation. EMBO Rep 14:206–211. https://doi.org/10.1038/embor.2012.208
57. Otomo C, Metlagel Z, Takaesu G, Otomo T. 2013. Structure of the human ATG12~ATG5 conjugate required for LC3 lipidation in autophagy. Nat Struct Mol Biol 20:59–66. https://doi.org/10.1038/nsmb.2431
58. Livak KJ, Schmittgen TD. 2001. Analysis of relative gene expression data using real-time quantitative PCR and the $2^{-\Delta\Delta CT}$ method. Methods 25:402–408. https://doi.org/10.1006/meth.2001.1262
59. Zhang J, Kennedy A, Xing L, Bui S, Reid W, Joppich J, Ahat E, Rose M, Tang Q, Tai AW, Wang Y. 2022. SARS-CoV-2 triggers Golgi fragmentation via down-regulation of GRASP55 to facilitate viral trafficking. bioRxiv. https://doi.org/10.1101/2022.03.04.483074
60. Atik N, Wirawan F, Amalia R, Khairani AF, Pradini GW. 2022. Differences in endosomal Rab gene expression between positive and negative COVID-19 patients. BMC Res Notes 15:252. https://doi.org/10.1186/s13104-022-06144-7
61. Kirchhausen T. 2000. Clathrin. Annu Rev Biochem 69:699–727. https://doi.org/10.1146/annurev.biochem.69.1.699
62. Royle SJ. 2006. The cellular functions of clathrin. Cell Mol Life Sci 63:1823–1832. https://doi.org/10.1007/s00018-005-5587-0
63. Scott CC, Vacca F, Gruenberg J. 2014. Endosome maturation, transport and functions. Semin Cell Dev Biol 31:2–10. https://doi.org/10.1016/j.semcdb.2014.03.034
64. Nagano M, Toshima JY, Siekhaus DE, Toshima J. 2019. Rab5-mediated endosome formation is regulated at the *trans*-Golgi network. Commun Biol 2:419. https://doi.org/10.1038/s42003-019-0670-5
65. Hu B, Chan JF-W, Liu H, Liu Y, Chai Y, Shi J, Shuai H, Hou Y, Huang X, Yuen TT-T, Yoon C, Zhu T, Zhang J, Li W, Zhang AJ, Zhou J, Yuan S, Zhang B-Z, Yuen K-Y, Chu H. 2022. Spike mutations contributing to the altered entry preference of SARS-CoV-2 omicron BA.1 and BA.2. Emerg Microbes Infect 11:2275–2287. https://doi.org/10.1080/22221751.2022.2117098
66. Carabelli AM, Peacock TP, Thorne LG, Harvey WT, Hughes J, COVID-19 Genomics UK Consortium, Peacock SJ, Barclay WS, de Silva TI, Towers GJ, Robertson DL. 2023. SARS-CoV-2 variant biology: immune escape, transmission and fitness. Nat Rev Microbiol 21:162–177. https://doi.org/10.1038/s41579-022-00841-7
67. Zeng C, Evans JP, King T, Zheng YM, Oltz EM, Whelan SPJ, Saif L, Peeples ME, Liu SL. 2021. SARS-CoV-2 spreads through cell-to-cell transmission. bioRxiv:2021.06.01.446579. https://doi.org/10.1101/2021.06.01.446579
68. Qing E, Gallagher T. 2023. Adaptive variations in SARS-CoV-2 spike proteins: effects on distinct virus-cell entry stages. mBio 14:e0017123. https://doi.org/10.1128/mbio.00171-23
69. Gerber PP, Duncan LM, Greenwood EJ, Marelli S, Naamati A, Teixeira-Silva A, Crozier TW, Gabaev I, Zhan JR, Mulroney TE, Horner EC, Doffinger R, Willis AE, Thaventhiran JE, Protasio AV, Matheson NJ. 2022. A protease-activatable luminescent biosensor and reporter cell line for authentic SARS-CoV-2 infection. PLoS Pathog 18:e1010265. https://doi.org/10.1371/journal.ppat.1010265
70. Stuchell-Brereton MD, Skalicky JJ, Kieffer C, Karren MA, Ghaffarian S, Sundquist WI. 2007. ESCRT-III recognition by VPS4 ATPases. Nature 449:740–744. https://doi.org/10.1038/nature06172
71. Adell MAY, Migliano SM, Upadhyayula S, Bykov YS, Sprenger S, Pakdel M, Vogel GF, Jih G, Skillern W, Behrouzi R, Babst M, Schmidt O, Hess MW, Briggs JA, Kirchhausen T, Teis D. 2017. Recruitment dynamics of ESCRT-III and Vps4 to endosomes and implications for reverse membrane budding. Elife 6:e31652. https://doi.org/10.7554/eLife.31652
72. Adell MAY, Vogel GF, Pakdel M, Müller M, Lindner H, Hess MW, Teis D. 2014. Coordinated binding of Vps4 to ESCRT-III drives membrane neck constriction during MVB vesicle formation. J Cell Biol 205:33–49. https://doi.org/10.1083/jcb.201310114
73. Helms JB, Rothman JE. 1992. Inhibition by brefeldin A of a Golgi membrane enzyme that catalyses exchange of guanine nucleotide bound to ARF. Nature 360:352–354. https://doi.org/10.1038/360352a0
74. Barzilay E, Ben-Califa N, Hirschberg K, Neumann D. 2005. Uncoupling of brefeldin a-mediated coatomer protein complex-I dissociation from Golgi redistribution. Traffic 6:794–802. https://doi.org/10.1111/j.1600-0854.2005.00317.x
75. Hsu VW, Yang JS. 2009. Mechanisms of COPI vesicle formation. FEBS Lett 583:3758–3763. https://doi.org/10.1016/j.febslet.2009.10.056
76. Sáenz JB, Sun WJ, Chang JW, Li J, Bursulaya B, Gray NS, Haslam DB. 2009. Golgicide A reveals essential roles for GBF1 in Golgi assembly and function. Nat Chem Biol 5:157–165. https://doi.org/10.1038/nchembio.144
77. van der Linden L, van der Schaar HM, Lanke KHW, Neyts J, van Kuppeveld FJM. 2010. Differential effects of the putative GBF1 inhibitors golgicide A and AG1478 on enterovirus replication. J Virol 84:7535–7542. https://doi.org/10.1128/JVI.02684-09
78. Chen D, Zhao YG, Zhang H. 2022. Endomembrane remodeling in SARS-CoV-2 infection. Cell Insight 1:100031. https://doi.org/10.1016/j.cellin.2022.100031
79. Hagemeijer MC, Rottier PJM, de Haan CAM. 2012. Biogenesis and dynamics of the coronavirus replicative structures. Viruses 4:3245–3269. https://doi.org/10.3390/v4113245

80. Gordon DE, Jang GM, Bouhaddou M, Xu J, Obernier K, White KM, O'Meara MJ, Rezelj VV, Guo JZ, Swaney DL, et al. 2020. A SARS-CoV-2 protein interaction map reveals targets for drug repurposing. Nature 583:459–468. https://doi.org/10.1038/s41586-020-2286-9
81. Andersen KG, Rambaut A, Lipkin WI, Holmes EC, Garry RF. 2020. The proximal origin of SARS-CoV-2. Nat Med 26:450–452. https://doi.org/10.1038/s41591-020-0820-9
82. Lytras S, Xia W, Hughes J, Jiang X, Robertson DL. 2021. The animal origin of SARS-CoV-2. Science 373:968–970. https://doi.org/10.1126/science.abh0117
83. Voskarides K. 2022. SARS-CoV-2: tracing the origin, tracking the evolution. BMC Med Genomics 15:62. https://doi.org/10.1186/s12920-022-01208-w
84. Ellwanger JH, Chies JAB. 2021. Zoonotic spillover: understanding basic aspects for better prevention. Genet Mol Biol 44:e20200355. https://doi.org/10.1590/1678-4685-GMB-2020-0355
85. Belov GA, van Kuppeveld FJM. 2012. (+)RNA viruses rewire cellular pathways to build replication organelles. Curr Opin Virol 2:740–747. https://doi.org/10.1016/j.coviro.2012.09.006
86. Wong LH, Edgar JR, Martello A, Ferguson BJ, Eden ER. 2021. Exploiting connections for viral replication. Front Cell Dev Biol 9:640456. https://doi.org/10.3389/fcell.2021.640456
87. King JS. 2012. Autophagy across the eukaryotes: is *S. cerevisiae* the odd one out? Autophagy 8:1159–1162. https://doi.org/10.4161/auto.20527
88. Qu Y, Wang X, Zhu Y, Wang W, Wang Y, Hu G, Liu C, Li J, Ren S, Xiao MZX, Liu Z, Wang C, Fu J, Zhang Y, Li P, Zhang R, Liang Q. 2021. ORF3a-mediated incomplete autophagy facilitates severe acute respiratory syndrome coronavirus-2 replication. Front Cell Dev Biol 9:716208. https://doi.org/10.3389/fcell.2021.716208
89. Tabata K, Prasad V, Paul D, Lee J-Y, Pham M-T, Twu W-I, Neufeldt CJ, Cortese M, Cerikan B, Stahl Y, et al. 2021. Convergent use of phosphatidic acid for hepatitis C virus and SARS-CoV-2 replication organelle formation. Nat Commun 12:7276. https://doi.org/10.1038/s41467-021-27511-1
90. Stein MP, Feng Y, Cooper KL, Welford AM, Wandinger-Ness A. 2003. Human VPS34 and p150 are Rab7 interacting partners. Traffic 4:754–771. https://doi.org/10.1034/j.1600-0854.2003.00133.x
91. Patki V, Virbasius J, Lane WS, Toh BH, Shpetner HS, Corvera S. 1997. Identification of an early endosomal protein regulated by phosphatidylinositol 3-kinase. Proc Natl Acad Sci U S A 94:7326–7330. https://doi.org/10.1073/pnas.94.14.7326
92. Futter CE, Collinson LM, Backer JM, Hopkins CR. 2001. Human VPS34 is required for internal vesicle formation within multivesicular endosomes. J Cell Biol 155:1251–1264. https://doi.org/10.1083/jcb.200108152
93. Hackstadt T, Chiramel AI, Hoyt FH, Williamson BN, Dooley CA, Beare PA, de Wit E, Best SM, Fischer ER. 2021. Disruption of the Golgi apparatus and contribution of the endoplasmic reticulum to the SARS-CoV-2 replication complex. Viruses 13:1798. https://doi.org/10.3390/v13091798
94. Dias SSG, Soares VC, Ferreira AC, Sacramento CQ, Fintelman-Rodrigues N, Temerozo JR, Teixeira L, Nunes da Silva MA, Barreto E, Mattos M, de Freitas CS, Azevedo-Quintanilha IG, Manso PPA, Miranda MD, Siqueira MM, Hottz ED, Pão CRR, Bou-Habib DC, Barreto-Vieira DF, Bozza FA, Souza TML, Bozza PT. 2020. Lipid droplets fuel SARS-CoV-2 replication and production of inflammatory mediators. PLoS Pathog 16:e1009127. https://doi.org/10.1371/journal.ppat.1009127
95. Yuan S, Yan B, Cao J, Ye Z-W, Liang R, Tang K, Luo C, Cai J, Chu H, Chung TW-H, To KK-W, Hung IF-N, Jin D-Y, Chan JF-W, Yuen K-Y. 2021. SARS-CoV-2 exploits host DGAT and ADRP for efficient replication. Cell Discov 7:100. https://doi.org/10.1038/s41421-021-00338-2
96. Pagliari F, Marafioti MG, Genard G, Candeloro P, Viglietto G, Seco J, Tirinato L. 2020. ssRNA virus and host lipid rearrangements: is there a role for lipid droplets in SARS-CoV-2 infection? Front Mol Biosci 7:578964. https://doi.org/10.3389/fmolb.2020.578964
97. Wu KE, Fazal FM, Parker KR, Zou J, Chang HY. 2020. RNA-GPS predicts SARS-CoV-2 RNA residency to host mitochondria and nucleolus. Cell Syst 11:102–108. https://doi.org/10.1016/j.cels.2020.06.008
98. Flynn RA, Belk JA, Qi Y, Yasumoto Y, Wei J, Alfajaro MM, Shi Q, Mumbach MR, Limaye A, DeWeirdt PC, Schmitz CO, Parker KR, Woo E, Chang HY, Horvath TL, Carette JE, Bertozzi CR, Wilen CB, Satpathy AT. 2021. Discovery and functional interrogation of SARS-CoV-2 RNA-host protein interactions. Cell 184:2394–2411. https://doi.org/10.1016/j.cell.2021.03.012
99. Shang C, Liu Z, Zhu Y, Lu J, Ge C, Zhang C, Li N, Jin N, Li Y, Tian M, Li X. 2021. SARS-CoV-2 causes mitochondrial dysfunction and mitophagy impairment. Front Microbiol 12:780768. https://doi.org/10.3389/fmicb.2021.780768
100. Shin HJ, Lee W, Ku KB, Yoon GY, Moon HW, Kim C, Kim MH, Yi YS, Jun S, Kim BT, Oh JW, Siddiqui A, Kim SJ. 2024. SARS-CoV-2 aberrantly elevates mitochondrial bioenergetics to induce robust virus propagation. Signal Transduct Target Ther 9:125. https://doi.org/10.1038/s41392-024-01836-x
101. Walia K, Sharma A, Paul S, Chouhan P, Kumar G, Ringe R, Sharma M, Tuli A. 2024. SARS-CoV-2 virulence factor ORF3a blocks lysosome function by modulating TBC1D5-dependent Rab7 GTPase cycle. Nat Commun 15:2053. https://doi.org/10.1038/s41467-024-46417-2
102. Zhu Y, Feng F, Hu G, Wang Y, Yu Y, Zhu Y, Xu W, Cai X, Sun Z, Han W, Ye R, Qu D, Ding Q, Huang X, Chen H, Xu W, Xie Y, Cai Q, Yuan Z, Zhang R. 2021. A genome-wide CRISPR screen identifies host factors that regulate SARS-CoV-2 entry. Nat Commun 12:961. https://doi.org/10.1038/s41467-021-21213-4
103. van der Bliek AM, Redelmeier TE, Damke H, Tisdale EJ, Meyerowitz EM, Schmid SL. 1993. Mutations in human dynamin block an intermediate stage in coated vesicle formation. J Cell Biol 122:553–563. https://doi.org/10.1083/jcb.122.3.553
104. Oostra M, Hagemeijer MC, van Gent M, Bekker CPJ, te Lintelo EG, Rottier PJM, de Haan CAM. 2008. Topology and membrane anchoring of the coronavirus replication complex: not all hydrophobic domains of nsp3 and nsp6 are membrane spanning. J Virol 82:12392–12405. https://doi.org/10.1128/JVI.01219-08
105. Baliji S, Cammer SA, Sobral B, Baker SC. 2009. Detection of nonstructural protein 6 in murine coronavirus-infected cells and analysis of the transmembrane topology by using bioinformatics and molecular approaches. J Virol 83:6957–6962. https://doi.org/10.1128/JVI.00254-09
106. Clementz MA, Kanjanahaluethai A, O'Brien TE, Baker SC. 2008. Mutation in murine coronavirus replication protein nsp4 alters assembly of double membrane vesicles. Virology (Auckl) 375:118–129. https://doi.org/10.1016/j.virol.2008.01.018
107. Imbert I, Snijder EJ, Dimitrova M, Guillemot J-C, Lécine P, Canard B. 2008. The SARS-coronavirus PLnc domain of nsp3 as a replication/transcription scaffolding protein. Virus Res 133:136–148. https://doi.org/10.1016/j.virusres.2007.11.017
108. Almasy KM, Davies JP, Plate L. 2021. Comparative host interactomes of the SARS-CoV-2 nonstructural protein 3 and human coronavirus homologs. Mol Cell Proteomics 20:100120. https://doi.org/10.1016/j.mcpro.2021.100120
109. Kanjanahaluethai A, Chen Z, Jukneliene D, Baker SC. 2007. Membrane topology of murine coronavirus replicase nonstructural protein 3. Virology (Auckl) 361:391–401. https://doi.org/10.1016/j.virol.2006.12.009
110. Audhya A, Desai A, Oegema K. 2007. A role for Rab5 in structuring the endoplasmic reticulum. J Cell Biol 178:43–56. https://doi.org/10.1083/jcb.200701139
111. Eden ER, White IJ, Tsapara A, Futter CE. 2010. Membrane contacts between endosomes and ER provide sites for PTP1B-epidermal growth factor receptor interaction. Nat Cell Biol 12:267–272. https://doi.org/10.1038/ncb2026
112. Stuible M, Tremblay ML. 2010. In control at the ER: PTP1B and the down-regulation of RTKs by dephosphorylation and endocytosis. Trends Cell Biol 20:672–679. https://doi.org/10.1016/j.tcb.2010.08.013
113. Friedman JR, DiBenedetto JR, West M, Rowland AA, Voeltz GK. 2013. Endoplasmic reticulum–endosome contact increases as endosomes traffic and mature. Mol Biol Cell 24:1030–1040. https://doi.org/10.1091/mbc.e12-10-0733
114. Lee CA, Blackstone C. 2020. ER morphology and endo-lysosomal crosstalk: functions and disease implications. Biochim Biophys Acta Mol Cell Biol Lipids 1865:158544. https://doi.org/10.1016/j.bbalip.2019.158544
115. Rowland AA, Chitwood PJ, Phillips MJ, Voeltz GK. 2014. ER contact sites define the position and timing of endosome fission. Cell 159:1027–1041. https://doi.org/10.1016/j.cell.2014.10.023
116. Allison R, Lumb JH, Fassier C, Connell JW, Ten Martin D, Seaman MNJ, Hazan J, Reid E. 2013. An ESCRT-spastin interaction promotes fission of recycling tubules from the endosome. J Cell Biol 202:527–543. https://doi.org/10.1083/jcb.201211045
117. Hoyer MJ, Chitwood PJ, Ebmeier CC, Striepen JF, Qi RZ, Old WM, Voeltz GK. 2018. A novel class of ER membrane proteins regulates

er-associated endosome fission. Cell 175:254–265. https://doi.org/10.1016/j.cell.2018.08.030
118. Rocha N, Kuijl C, van der Kant R, Janssen L, Houben D, Janssen H, Zwart W, Neefjes J. 2009. Cholesterol sensor ORP1L contacts the ER protein VAP to control Rab7-RILP-p150 glued and late endosome positioning. J Cell Biol 185:1209–1225. https://doi.org/10.1083/jcb.200811005
119. Jongsma MLM, Berlin I, Wijdeven RHM, Janssen L, Janssen GMC, Garstka MA, Janssen H, Mensink M, van Veelen PA, Spaapen RM, Neefjes J. 2016. An ER-associated pathway defines endosomal architecture for controlled cargo transport. Cell 166:152–166. https://doi.org/10.1016/j.cell.2016.05.078
120. Raiborg C, Wenzel EM, Pedersen NM, Olsvik H, Schink KO, Schultz SW, Vietri M, Nisi V, Bucci C, Brech A, Johansen T, Stenmark H. 2015. Repeated ER-endosome contacts promote endosome translocation and neurite outgrowth. Nature 520:234–238. https://doi.org/10.1038/nature14359
121. Haj FG, Verveer PJ, Squire A, Neel BG, Bastiaens PIH. 2002. Imaging sites of receptor dephosphorylation by PTP1B on the surface of the endoplasmic reticulum. Science 295:1708–1711. https://doi.org/10.1126/science.1067566
122. Atakpa P, Thillaiappan NB, Mataragka S, Prole DL, Taylor CW. 2018. IP3 receptors preferentially associate with ER-lysosome contact sites and selectively deliver Ca^{2+} to lysosomes. Cell Rep 25:3180–3193. https://doi.org/10.1016/j.celrep.2018.11.064
123. de Wilde AH, Wannee KF, Scholte FEM, Goeman JJ, Ten Dijke P, Snijder EJ, Kikkert M, van Hemert MJ. 2015. A kinome-wide small interfering RNA screen identifies proviral and antiviral host factors in severe acute respiratory syndrome coronavirus replication, including double-stranded RNA-activated protein kinase and early secretory pathway proteins. J Virol 89:8318–8333. https://doi.org/10.1128/JVI.01029-15
124. Tiwari R, Mishra AR, Gupta A, Nayak D. 2022. Structural similarity-based prediction of host factors associated with SARS-CoV-2 infection and pathogenesis. J Biomol Struct Dyn 40:5868–5879. https://doi.org/10.1080/07391102.2021.1874532
125. Pérez-Pulido AJ, Asencio-Cortés G, Brokate-Llanos AM, Brea-Calvo G, Rodríguez-Griñolo R, Garzón A, Muñoz MJ. 2021. Serial co-expression analysis of host factors from SARS-CoV viruses highly converges with former high-throughput screenings and proposes key regulators. Brief Bioinform 22:1038–1052. https://doi.org/10.1093/bib/bbaa419
126. Ewald SE, Lee BL, Lau L, Wickliffe KE, Shi GP, Chapman HA, Barton GM. 2008. The ectodomain of Toll-like receptor 9 is cleaved to generate a functional receptor. Nature 456:658–662. https://doi.org/10.1038/nature07405
127. Park B, Brinkmann MM, Spooner E, Lee CC, Kim YM, Ploegh HL. 2008. Proteolytic cleavage in an endolysosomal compartment is required for activation of Toll-like receptor 9. Nat Immunol 9:1407–1414. https://doi.org/10.1038/ni.1669
128. Brencicova E, Diebold SS. 2013. Nucleic acids and endosomal pattern recognition: how to tell friend from foe? Front Cell Infect Microbiol 3:37. https://doi.org/10.3389/fcimb.2013.00037
129. Imam S, Talley S, Nelson RS, Dharan A, O'Connor C, Hope TJ, Campbell EM. 2016. TRIM5α degradation via autophagy is not required for retroviral restriction. J Virol 90:3400–3410. https://doi.org/10.1128/JVI.03033-15
130. Sanjana NE, Shalem O, Zhang F. 2014. Improved vectors and genome-wide libraries for CRISPR screening. Nat Methods 11:783–784. https://doi.org/10.1038/nmeth.3047
131. Shi Y, Simpson S, Ahmed SK, Chen Y, Tavakoli-Tameh A, Janaka SK, Evans DT, Serra-Moreno R. 2023. The antiviral factor SERINC5 impairs the expression of non-self-DNA. Viruses 15:1961. https://doi.org/10.3390/v15091961
132. Shi Y, Simpson S, Chen Y, Aull H, Benjamin J, Serra-Moreno R. 2024. Mutations accumulated in the spike of SARS-CoV-2 Omicron allow for more efficient counteraction of the restriction factor BST2/Tetherin. PLoS Pathog 20:e1011912. https://doi.org/10.1371/journal.ppat.1011912
133. Itakura E, Mizushima N. 2010. Characterization of autophagosome formation site by a hierarchical analysis of mammalian Atg proteins. Autophagy 6:764–776. https://doi.org/10.4161/auto.6.6.12709
134. Votteler J, Ogohara C, Yi S, Hsia Y, Nattermann U, Belnap DM, King NP, Sundquist WI. 2016. Designed proteins induce the formation of nanocage-containing extracellular vesicles. Nature 540:292–295. https://doi.org/10.1038/nature20607
135. Vonderheit A, Helenius A. 2005. Rab7 associates with early endosomes to mediate sorting and transport of Semliki forest virus to late endosomes. PLoS Biol 3:e233. https://doi.org/10.1371/journal.pbio.0030233
136. Castro-Gonzalez S, Shi Y, Colomer-Lluch M, Song Y, Mowery K, Almodovar S, Bansal A, Kirchhoff F, Sparrer K, Liang C, Serra-Moreno R. 2021. HIV-1 Nef counteracts autophagy restriction by enhancing the association between BECN1 and its inhibitor BCL2 in a PRKN-dependent manner. Autophagy 17:553–577. https://doi.org/10.1080/15548627.2020.1725401
137. Shi Y, Castro-Gonzalez S, Chen Y, Serra-Moreno R. 2021. Effects of the SUMO ligase BCA2 on metabolic activity, cell proliferation, cell migration, cell cycle, and the regulation of NF-κB and IRF1 in different breast epithelial cellular contexts. Front Cell Dev Biol 9:711481. https://doi.org/10.3389/fcell.2021.711481
138. Colomer-Lluch M, Serra-Moreno R. 2017. BCA2/Rabring7 interferes with HIV-1 proviral transcription by enhancing the SUMOylation of IκBα. J Virol 91:e02098-16. https://doi.org/10.1128/JVI.02098-16
139. Ramakrishnan MA. 2016. Determination of 50% endpoint titer using a simple formula. World J Virol 5:85–86. https://doi.org/10.5501/wjv.v5.i2.85